

Assessment of uranium nitride interatomic potentials

Mohamed AbdulHameed^a, Benjamin Beeler^{a,b,*}, Conor O.T. Galvin^c, Michael W.D. Cooper^c

^a*Department of Nuclear Engineering, North Carolina State University, Raleigh, NC 27695*

^b*Idaho National Laboratory, Idaho Falls, ID 83415*

^c*Los Alamos National Laboratory, Los Alamos, NM 87545*

Abstract

Uranium mononitride (UN) is a promising nuclear fuel due to its high fissile density, high thermal conductivity, and suitability for reprocessing. In this study, two uranium nitride interatomic potentials are assessed: Tseplyaev and Starikov's angular-dependent potential and Kocevski *et al.*'s embedded atom model potential. Predictions of the thermophysical and elastic properties of UN, UN₂, and α - and β -U₂N₃ computed using both potentials are assessed and compared to available experimental data. The Tseplyaev potential performs better with the energetic aspects of UN, e.g., specific heat capacity and point defect formation energies, whereas the Kocevski potential performs better with the structural aspects of UN, e.g., thermal expansion as well as with the elastic properties. The reasons why the Kocevski potential underestimates the UN specific heat are explained by examining the UN phonon properties modeled using both potentials. The Kocevski potential shows better identification of the mechanical stability ranges of UN, UN₂, and α - and β -U₂N₃, reasonably predicting the melting point of UN and predicting stable structures for UN₂ and α - and β -U₂N₃. On the other hand, the Tseplyaev potential predicts a premature phase change of both UN and UN₂ and cannot stabilize α - nor β -U₂N₃. However, the Kocevski potential cannot predict a stable α -U phase and is thus not suitable for the calculation of formation energies for non-stoichiometric point defects.

Keywords: uranium nitride, thermophysical properties, molecular dynamics, phonons, point defects

1. Introduction

Since the 2011 Fukushima Daiichi accident in Japan, research efforts have been directed to develop advanced nuclear fuels that have improved performance in extreme conditions compared to UO₂ while maintaining thermodynamic and mechanical stability [1]. One such fuel candidate is uranium mononitride (UN), which has shown many positive characteristics including high fissile density, high thermal conductivity, good dissolution in nitric acid making it compatible with the PUREX process, good chemical compatibility with most potential cladding materials, and longer fuel residence time [2, 3, 4]. However, it has also

*Corresponding author

Email address: bwbeeler@ncsu.edu (Benjamin Beeler)

9 suffered some drawbacks that historically hindered its industrial adoption, including com-
10 plicated fabrication processes, high fuel cost owing to the need for N-15 enrichment, low
11 resistance to oxidation by high-temperature steam, and high swelling rates [2, 3, 4].

12 UN has not been investigated as widely as oxide fuels, and many aspects of its behavior
13 at high temperatures and under irradiation are not well understood [5]. To address its
14 drawbacks and build a case for its practical use in light-water and advanced reactors, UN
15 properties should be well-understood at the atomic and mesoscales. Multiscale multiphysics
16 fuel performance models can provide a pathway for the descriptive and predictive evolution
17 of nuclear fuels and are especially valuable in cases where experimental data is limited. These
18 models, however, require many input parameters from lower-length scale simulation methods
19 like density functional theory (DFT) and molecular dynamics (MD).

20 Many DFT studies have been conducted on UN to predict its electronic structure and
21 magnetic ordering [6, 7, 8, 9, 10] as well as to understand the properties of its point de-
22 fects [11, 12, 13, 14], impurities [15], and fission products [16, 17, 18, 19]. However, DFT is
23 computationally demanding and has limitations in system size and simulation time. MD sim-
24 ulations can overcome these limitations and offer more flexibility in predicting fuel behavior
25 at finite temperatures. Still, the accuracy of MD results is highly dependent on the quality
26 of the interatomic potentials employed. Therefore, a reliable UN interatomic potential is a
27 necessity.

28 For UN, several interatomic potentials exist in the literature. Kurosaki *et al.* [20, 21] de-
29 veloped a Busing-Ida type potential which they used to predict thermal expansion, constant-
30 pressure specific heat capacity, and thermal conductivity. Calculated properties qualitatively
31 agree with experimental results at low temperatures and exhibit an increasing underestima-
32 tion with increasing temperature. Kurosaki *et al.* mention the values of potential parameters
33 without units, which makes it hard to further assess its behavior. Chen *et al.* [22] used the
34 Chen–Möbius lattice inversion method to derive three Morse-type pair potentials for the
35 U-U, N-N, and U-N interactions. The potential was then used to predict thermal expansion
36 and compressibility with a moderate qualitative agreement. However, Morse-type potentials
37 cannot capture the nature of atomic bonding, especially in covalent solids such as UN [23].

38 Kuksin *et al.* [24] developed an angular-dependent potential (ADP) fitted to DFT calcu-
39 lations. The potential was modified in a later paper by Tseplyaev and Starikov [25], and used
40 to calculate point defect formation and migration energies and to predict the UN pressure-
41 induced $Fm\bar{3}m \rightarrow R\bar{3}m$ phase transition. However, the authors didn't consider the effect of
42 stoichiometry on defect formation energies, and their methodology to calculate the U and
43 N chemical potentials is not reported. They also show evidence of the potential's capability
44 to predict some basic properties of UN_2 and U_2N_3 . Li and Murphy [26] have later used this
45 potential to study self-diffusion in hypo-stoichiometric UN.

46 Kocevski *et al.* [27] developed an embedded-atom method (EAM) potential fitted to
47 experimental thermal expansion and single crystal elastic constants, as well as formation
48 energies of stoichiometric point defects from DFT calculations. The potential was used
49 to calculate the elastic properties and temperature-dependent heat capacity. However, the
50 authors assumed UN to be an isotropic material, which is not true as will be explained in
51 3.3, and the heat capacity was underestimated at high temperatures. Also, the potential
52 was used to study Xe diffusion in UN.

53 Tseplyaev and Starikov's ADP (hereafter referred to as the Tseplyaev potential) and Ko-

54 cevski *et al.*'s EAM potential (hereafter referred to as the Kocevski potential) are promising
 55 candidate potentials by their construction that attempts to model the complex bonding en-
 56 vironment of UN. The main goal of this work is to assess the performance of both potentials
 57 and to identify their relevant artifacts and weaknesses by performing MD simulations that
 58 calculate UN elastic properties, specific heat capacity, and phonon properties. We also cal-
 59 culate point defect formation energies using a methodology that removes the arbitrariness in
 60 chemical potential determination. Thermophysical and elastic properties of UN_2 and U_2N_3
 61 phases are also computed, and their predicted stability is discussed.

62 2. Computational details

63 All MD calculations performed in this work utilize the Large-scale Atomic/Molecular
 64 Massively Parallel Simulator (LAMMPS) software package [28] with a time step of 1 fs
 65 and periodic boundary conditions applied in all directions. The Phonopy code [29] is used
 66 to calculate phonon properties. To obtain the forces calculated by LAMMPS in a format
 67 readable by Phonopy, PhonoLAMMPS, an auxiliary tool of the DynaPhoPy code [30], is
 68 used. Detailed computational methodologies of all properties are presented in the respective
 69 sections.

70 2.1. Structural properties

71 The U-N solid system has three distinct compounds: UN, uranium dinitride (UN_2), and
 72 uranium sesquinitride (U_2N_3) [31]. UN has a NaCl crystal structure with a lattice parameter
 73 $a = 4.89 \text{ \AA}$ at room temperature [32] and a melting temperature $T_m = 3035 \text{ K}$ at a nitrogen
 74 vapor pressure of 1 atm [33]. UN_2 has a fluorite crystal structure with an experimental
 75 lattice parameter $a = 5.21 \text{ \AA}$ [34]. U_2N_3 has a bixbyite crystal structure at low temperatures
 76 ($\alpha\text{-U}_2\text{N}_3$) and a hexagonal crystal structure at high temperatures ($\beta\text{-U}_2\text{N}_3$) [4]. $\alpha\text{-U}_2\text{N}_3$ has
 77 a space group: $Ia\bar{3}$, and a lattice parameter of 10.7 \AA , whereas $\beta\text{-U}_2\text{N}_3$ has a space group:
 78 $P\bar{3}m1$, Pearson symbol: $hP5$, and lattice parameters: $a = 3.69 \text{ \AA}$, $c = 5.83 \text{ \AA}$, $z_U = 0.2467$,
 79 and $z_N = 0.6470$ [35, 36]. UN_x has the fluorite crystal structure in the composition range
 80 of $1.75 \leq x \leq 2.00$, whereas the $\text{UN}_2/\alpha\text{-U}_2\text{N}_3$ solid solution is stable for $1.54 \leq x \leq 1.75$
 81 [31]. Additionally, the conventional unit cell of $\alpha\text{-U}_2\text{N}_3$ can be regarded as a $2 \times 2 \times 2$
 82 UN_2 supercell with a quarter of the N atoms removed [37]. For these reasons, the names
 83 UN and U_2N_3 are often used interchangeably to refer to the $\text{UN}_2/\alpha\text{-U}_2\text{N}_3$ solid solution at
 84 low and intermediate temperatures [31, 4]. The $\text{UN}_2/\alpha\text{-U}_2\text{N}_3$ solid solution decomposes at a
 85 temperature of either 1324 K [4] or 1405 K [38], the uncertainty being due to the dependence
 86 of the U-N phase diagram on the nitrogen vapor pressure [4]. Due to the same uncertainty,
 87 $\beta\text{-U}_2\text{N}_3$ exists as a single phase in either the temperature range 1324-1648 K [4] or the range
 88 1214-1625 K [38].

89 We compare the UN lattice constant predicted by both potentials through 0 K energy
 90 minimization to the experimental value. The UN linear thermal expansion coefficient (LTEC)
 91 predicted by both potentials is also computed. To allow comparison with the Hayes *et al.*
 92 [32] empirical correlation, the mean LTEC is defined as (assuming isotropic expansion):

$$\alpha_L = \frac{a - a_0}{a_0(T - T_0)} \quad (1)$$

93 where a is the lattice parameter and a_0 is the lattice parameter at a reference temperature
94 $T_0 = 300$ K. It should be noted that this definition of the LTEC is different from the
95 thermodynamic definition: $\alpha_L = (1/a)\partial a/\partial T$. To calculate the temperature variation of the
96 lattice parameters and LTECs of UN, UN_2 , α - and β - U_2N_3 , $15 \times 15 \times 15$ supercells of UN,
97 UN_2 , and α - U_2N_3 (and $8 \times 8 \times 8$ supercells of β - U_2N_3) are equilibrated in the *NPT* ensemble
98 for 100 ps and their lattice parameters are averaged over the last 50 ps. Unless otherwise
99 stated, these supercell sizes are used in all subsequent calculations.

100 *2.2. Melting point*

101 The thermodynamic definition of melting is the point at which solid and liquid states co-
102 exist, and thus have the same free energy [39, 40]. However, the melting point predicted by
103 MD based on simple heating corresponds to the point at which the solid lattice mechanically
104 collapses, and is usually overestimated compared to the true one due to the existence of a free
105 energy barrier to the formation of a solid-liquid interface in perfect supercells. This barrier
106 leads to a hysteresis effect associated with the necessity to run the simulation for a sufficient
107 time at a superheated temperature so that a seed of the liquid phase can spontaneously nu-
108 cleate [41, 39]. This free-energy barrier can be eliminated by using the void-induced melting
109 method [39, 40]. Voids (introduced in the supercell in the form of Schottky defects) form local
110 pockets of a liquid-like structure, which effectively introduces solid-liquid interfaces. With
111 increasing the number of voids, the free energy barrier to melting decreases, until, for a
112 sufficient number of voids, the predicted melting point reaches a plateau for a limited range.
113 If too many voids are introduced, the solid becomes mechanically unstable and collapses
114 without a discontinuous solid-to-liquid phase transition [39]. Melting is a first-order phase
115 transition that is signified by a step-like transition in the volume versus temperature curve,
116 or, equivalently, a spike in the specific heat versus temperature curve [42]. Voids within the
117 range 0-2 at. % are introduced into the UN supercells, which are then equilibrated in the
118 *NPT* ensemble for 100 ps, their total energy and volume are averaged over the last 50 ps,
119 and the solid-to-liquid transition temperatures are recorded for each vacancy concentration.

120 *2.3. Elastic properties*

121 The elastic stiffness tensor, C_{ij} , is computed using the explicit deformation method [43].
122 At 0 K, supercells of UN, UN_2 , α - and β - U_2N_3 are relaxed and then strains are applied
123 to the $\pm x$ -, $\pm y$ -, and $\pm z$ -directions with magnitudes of 0.005%, 0.01%, and 0.05%. The
124 supercell energy is minimized with a constant volume and the stress tensor is calculated.
125 For the finite-temperature calculations, averaged UN and UN_2 lattice parameters at each
126 temperature are used to construct supercells of the same size, whereas, for α - and β - U_2N_3 ,
127 the supercells are initially equilibrated in the *NPT* ensemble for 50 ps. Supercells are then
128 equilibrated for 20 ps using a Langevin thermostat, the Langevin thermostat is then switched
129 off and strains of 0.5%, 0.1%, and 1.5% are applied to the same directions under the *NVE*
130 ensemble. Finally, the stress tensor components are then averaged over the next 10 ps. For
131 the UN, UN_2 , and α - U_2N_3 crystals with cubic symmetry, only three of the elastic constants
132 are independent: C_{11} , C_{12} , and C_{44} [44], whereas, for the hexagonal structure of β - U_2N_3 , five
133 elastic constants are independent: C_{11} , C_{12} , C_{13} , C_{33} and C_{44} [45]. Various strains are used
134 at 0 K and finite temperatures to make sure the elastic properties are strain-independent.

¹³⁵ Larger strains are used at finite temperatures to reduce uncertainties arising from thermal
¹³⁶ fluctuations.

¹³⁷ Polycrystalline elastic moduli are computed from the single-crystal elastic constants ac-
¹³⁸ cording to the Voigt-Reuss-Hill (VRH) approach [46, 44, 43] as Hill averages of upper Voigt
¹³⁹ limits and lower Reuss limits on the bulk and shear moduli. The form of the VRH elastic
¹⁴⁰ moduli is included in [Appendix A](#). The elastic stability criteria are also checked for UN, UN₂,
¹⁴¹ and α - and β -U₂N₃. For cubic crystals, the conditions for elastic stability are $C_{11} - C_{12} > 0$,
¹⁴² $C_{11} + 2C_{12} > 0$, and $C_{44} > 0$, whereas, for hexagonal crystals, the elastic stability conditions
¹⁴³ are: $C_{11} > |C_{12}|$, $2C_{13}^2 < C_{33}(C_{11} + C_{12})$, and $C_{44} > 0$ [47]. The stability of the solid crystal
¹⁴⁴ structure is also judged by observing the radial distribution functions (RDFs) calculated
¹⁴⁵ by OVITO. For a specific crystal structure, the RDF is characterized by distinct peaks. A
¹⁴⁶ phase transformation to a different crystal structure is characterized by the change of peak
¹⁴⁷ positions, whereas for a liquid, the RDF is characterized by a single peak after which the
¹⁴⁸ RDF assumes a value of about 1 [48].

¹⁴⁹ The Anderson method is one of the standard methods to calculate the Debye temperature
¹⁵⁰ from the 0 K elastic constants according to the equations [46]:

$$\theta_D = \frac{h}{k_B} \left(\frac{3q}{4\pi} \frac{N_A \rho}{M} \right)^{1/3} v_0 \quad (2)$$

$$v_0 = \left[\frac{1}{3} \left(\frac{2}{v_t^3} + \frac{1}{v_l^3} \right) \right]^{-1/3} \quad (3)$$

$$v_t = \sqrt{\frac{G}{\rho}} \quad (4)$$

$$v_l = \sqrt{\frac{3B + 4G}{3\rho}} \quad (5)$$

¹⁵⁴ where q is the number of atoms per formula unit ($q = 2$ for UN), M is the molecular weight,
¹⁵⁵ v_0 is the average sound velocity, v_t is the average transverse sound velocity for an isotropic
¹⁵⁶ material, and v_l is the average longitudinal sound velocity for an isotropic material. Another
¹⁵⁷ method to calculate the Debye temperature for cubic crystals is the semi-empirical Siethoff-
¹⁵⁸ Ahlborn method based on the room-temperature elastic constants [49]:

$$\theta_D = C \left(\frac{aqG'}{M} \right)^{1/2} \quad (6)$$

$$G' = \left[C_{44} \left(\frac{(C_{11} - C_{12})C_{44}}{2} \right)^{1/2} \left(\frac{C_{11} - C_{12} + C_{44}}{3} \right) \right]^{1/3} \quad (7)$$

¹⁶⁰ where a is the lattice constant, and C is an empirical parameter that depends on the crystal
¹⁶¹ structure ($C = 18.56$ K for the NaCl structure). q and M have the same meaning as in the
¹⁶² Anderson method. Both methods are utilized for the determination of θ_D in this work.

163 2.4. Specific heat capacity

164 Because UN behaves as a metallic solid [19, 50], its constant-pressure specific heat ca-
 165 pacity, C_P , has two main contributions: lattice, C_{lat} , and electronic, C_{elec} , specific heat
 166 capacities, where electron-phonon interactions have been neglected. To calculate C_{lat} , su-
 167 percells are equilibrated in the NPT ensemble for 100 ps and their total energy is averaged
 168 over the last 50 ps. All specific heats are computed as the slope of the potential energy as a
 169 function of temperature using three-point centered finite differences with 50 K increments.
 170 C_{lat} can be decomposed into the following contributions [51, 52]:

$$C_{\text{lat}} = C_V + C_{\text{exp}} + C_{\text{anharm}} + C_d \quad (8)$$

171 where C_V is the constant-volume specific heat, C_{exp} is the contribution due to thermal
 172 expansion, C_{anharm} is the anharmonic non-expansive contribution, and C_d is the contribution
 173 due to defect generation. C_V is calculated by restricting the supercells to the equilibrium 0
 174 K volume and averaging the total energy within the NVT ensemble. C_{exp} can be calculated
 175 from [53]:

$$C_{\text{exp}} = 9\alpha_L^2 BV_m T \quad (9)$$

176 where α_L is the linear thermal expansion coefficient, B is the bulk modulus, and V_m is the
 177 molar volume. Neglecting C_d for perfect crystals, C_{anharm} (Fig. 4d) is calculated from:

$$C_{\text{anharm}} = C_{\text{lat}} - C_V - C_{\text{exp}} \quad (10)$$

178 C_{elec} is estimated from [54, 20, 50]:

$$C_{\text{elec}} = \frac{\pi}{3} g(\epsilon_F) N_A k_B^2 T = \gamma T \quad (11)$$

179 where $g(\epsilon_F)$ is the density of states (DOS) at the Fermi level (states/eV-atom), and γ is the
 180 electronic specific heat coefficient (J/mol-K²). Samsel-Czeała *et al.* [6] reported a value of γ
 181 = 3.7 mJ/mol-K² based on their electronic-structure calculation, and this is the value used in
 182 our calculations. Kocevski *et al.* [50] reported $g(\epsilon_F) = 2$ -2.2 states/eV-atom in their *ab initio*
 183 MD calculation, which gives a value of γ equal to about 1.5-1.7 mJ/mol-K². These γ values
 184 are in large contrast with the experimentally reported values of about 34 mJ/mol-K² [55]
 185 and 50 mJ/mol-K² [56] obtained by fitting heat capacity data. Szpunar *et al.* [57] have also
 186 calculated γ using the Quantum ESPRESSO code and found $\gamma = 17.6$ mJ/mol-K² for the
 187 PBEsol functional and $\gamma = 0.6$ mJ/mol-K² for the non-local hybrid B3LYP functional–both
 188 values being smaller than the experimental ones.

189 2.5. Phonon properties

190 To get a deeper understanding of the calculated thermal properties of UN, we study how
 191 the Tseplyaev and Kocevski potentials model the UN phonon properties. Harmonic force
 192 constants are calculated using the finite displacement method [58]. To compute accurate
 193 forces using small displacements, initial UN structures must be fully relaxed [59], which was
 194 accomplished using static energy minimization in LAMMPS. The equilibrium UN lattice
 195 constants of each potential are then used to construct $3 \times 3 \times 3$ UN *primitive* cells (54
 196 atoms). PhonoLAMMPS, coupled to LAMMPS, is used to apply a displacement of 0.01 Å

¹⁹⁷ to the supercell and get the interatomic forces of the displaced configurations, where the
¹⁹⁸ required displacement patterns are determined by the symmetry of the supercell. Phonopy
¹⁹⁹ reads the generated forces and calculates symmetrized harmonic force constants from [60, 61]:

$$K_{ls\alpha,l's'\beta} = -\frac{\partial F_{ls\alpha}}{\partial u_{l's'\beta}} \quad (12)$$

²⁰⁰ where $K_{ls\alpha,l's'\beta}$ is a second-order (harmonic) force constant, l labels the unit cells, s labels the
²⁰¹ atoms within each unit cell, α and β label Cartesian coordinates, $u_{l's'\beta}$ is the displacement of
²⁰² atom s' within unit cell l' in the β direction and the force $F_{ls\alpha} = -\partial U / \partial u_{ls\alpha}$ where U is the
²⁰³ lattice potential energy. The phonon band structure is calculated along the high symmetry
²⁰⁴ k -path: Γ - X - K - Γ - L to allow comparison with experimental results. To compute the phonon
²⁰⁵ DOS, the reciprocal space is sampled by a Γ -centered $100 \times 100 \times 100$ mesh, and the linear
²⁰⁶ tetrahedron method is used for integration in the Brillouin zone.

²⁰⁷ 2.6. Point defect formation energies

²⁰⁸ The formation energy of uncharged point defects at $T = 0$ K is defined as [62, 63, 64]:

$$E_f = E_d - E_p - \sum_i n_i \mu_i = \delta E - \sum_i n_i \mu_i \quad (13)$$

²⁰⁹ where E_d and E_p are the energies of the defective and perfect supercells, respectively, n_i is
²¹⁰ the number of atoms of type i removed ($n_i < 0$) or added ($n_i > 0$) to form the defect, and
²¹¹ μ_i is the chemical potential of the i th species. δE is termed the “raw” formation energy [62].
²¹² For Schottky defects (SD) and Frenkel defects (FD), the crystal’s stoichiometry does not
²¹³ change, and special cases of Eq. (13) exist. For Frenkel defects, the formation energy is just
²¹⁴ $E_f = E_d - E_p$, whereas, for a Schottky defect, the formation energy is:

$$E_f = E_d - \frac{N - A}{N} E_p \quad (14)$$

²¹⁵ where N is the total number of atoms in the supercell, and A is the number of atoms per
²¹⁶ formula unit ($A = 2$ for UN) [65].

²¹⁷ Chemical potentials represent the energy of the reservoirs with which atoms are being
²¹⁸ exchanged [63, 66], and the proper choice of the chemical potentials in Eq. (13) depends on
²¹⁹ phase stabilities of the considered system [66]. For a binary compound AB, the chemical
²²⁰ potentials of A and B vary from A-rich to B-rich compositions displaying a discontinuity at
²²¹ the stoichiometric composition [67, 62, 68]. While numerous formalisms exist in the literature
²²² for determining the chemical potentials of relevant species [62, 13, 67, 68, 63, 27], the method
²²³ of Huang *et al.* [69, 19] is used in this work. In this method, upper and lower bounds are
²²⁴ imposed on the chemical potential to capture its dependence on stoichiometry; these bounds
²²⁵ are dictated by the cohesive energies of the competing phases at very low temperatures.
²²⁶ Based on an examination of the UN phase diagram [38, 4], it can be argued that the bounds
²²⁷ on the U and N chemical potentials at very low temperatures are governed by transformations
²²⁸ to α -U for U-rich conditions (i.e., co-existence of UN and α -U), and transformation to UN₂
²²⁹ for N-rich conditions (i.e., co-existence of UN and UN₂) [69, 19]. Accordingly, the U and N
²³⁰ chemical potentials are calculated from [19]:

$$E_c(\text{U}_x\text{N}_y) = x\mu_{\text{U}} + y\mu_{\text{N}} \quad (15)$$

where $E_c(U_xN_y)$ is the cohesive energy (energy per formula unit). Eq. (15) is solved for UN and α -U to get the U-rich chemical potentials, and for UN and UN_2 to get the N-rich chemical potentials [69, 19]. The chemical potentials at stoichiometric conditions are the averages of these two bounds [68].

Although many DFT studies have investigated point defect formation energies in UN [11, 13, 14, 24, 25, 27], only Yang and Kaltsoyannis [19] and Kocevski *et al.* [10] have looked at their variation with stoichiometry. Yang and Kaltsoyannis used the PW91 functional, whereas Kocevski *et al.* used the PBE and AM05 functionals, with and without an added on-site Coulomb repulsion term ($+U$), and found a variation of the defect formation energies with different DFT methodologies.

3. Results

3.1. Structural properties

The UN lattice parameters predicted by the Tseplyaev and Kocevski potentials at 0 K are 4.81 Å and 4.90 Å, respectively, compared to the experimental room temperature (RT) value of 4.89 Å [32]. As can be seen in Fig. 1a, the Kocevski potential is closer in comparison to the experimental results of both Hayes *et al.* [32] and Liu *et al.* [70], whereas the Tseplyaev potential slightly underestimates it. The linear thermal expansion coefficient (LTEC) is shown in Fig. 1b. The Tseplyaev potential predicts a temperature-independent thermal expansion up to about 1000 K and then predicts a fifth-order power-law expansion—a trend that does not agree with experimental observations. On the other hand, while the Kocevski potential underestimates the UN LTEC with a larger error than that of the Tseplyaev potential, it predicts a trend very similar to that given by Hayes *et al.* and Liu *et al.* This is in accordance with the recently published results from Galvin *et al.* [71].

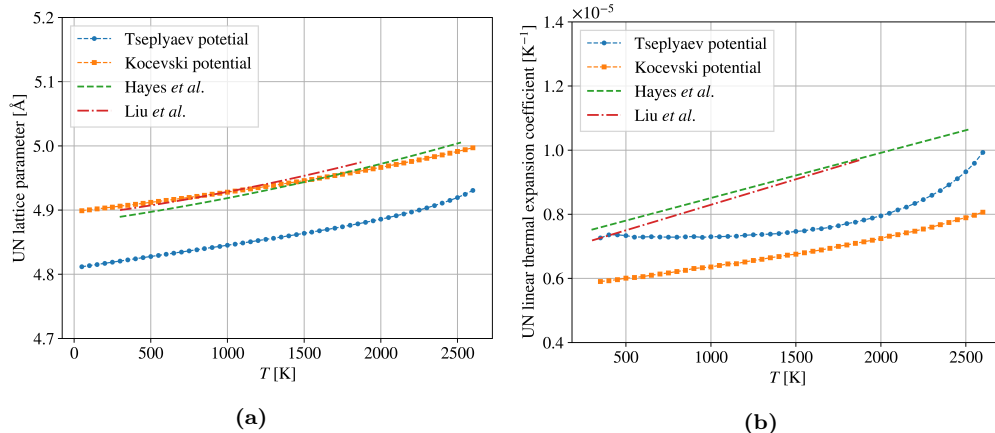


Figure 1: (a) UN lattice parameter calculated by both potentials and compared to the experimental data of Hayes *et al.* [32] and Liu *et al.* [70]. (b) UN linear thermal expansion coefficient calculated by both potentials and compared to the experimental data of Hayes *et al.* [32] and Liu *et al.* [70].

3.2. Melting point

The melting temperature predicted by both potentials is shown in Fig. 2. According to Alavi and Thompson [39], the thermodynamic melting point is determined as the value of

the range over which the melting temperature appears to be independent of the vacancy concentration. Based on this measure, the Tseplyaev potential predicts thermodynamic melting at about 2700 K, whereas the Kocevski potential predicts it at about 3100 K; a value that is close to the experimental value of 3035 K estimated from the Hayes *et al.* correlation at a nitrogen vapor pressure of 1 atm [33]. It can be concluded that the Kocevski potential gives a better prediction of the phase stability range of UN because its predicted melting point is closer to the experimental data, whereas the Tseplyaev potential predicts a slightly premature melting of UN.

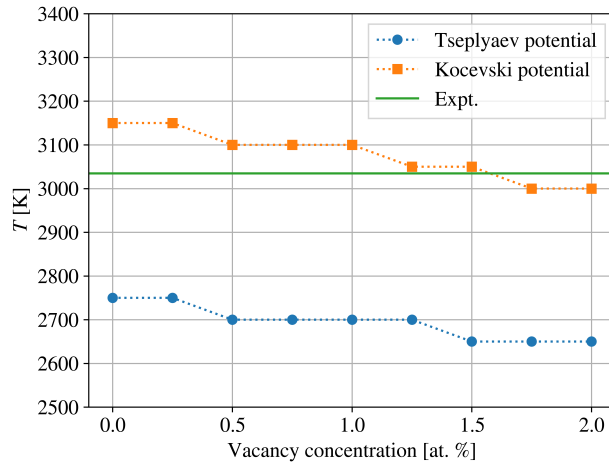


Figure 2: UN melting point as predicted by both potentials as a function of vacancy concentration using the void-induced melting method. The experimental melting temperature (3035 K) is taken from the Hayes *et al.* correlation at a nitrogen vapor pressure of 1 atm [33].

3.3. Elastic properties

The UN elastic constants calculated at 0 K using both potentials are shown in Table 1. A much larger error is associated with the values of C_{11} and C_{44} calculated by the Tseplyaev potential compared to those calculated by the Kocevski potential, whereas the Tseplyaev potential estimation of C_{12} is slightly better. It was found that UN elastic constants calculated at 0 K using the Tseplyaev potential show a discontinuity compared to finite-temperature values, which contradicts the third law of thermodynamics that requires a near-zero slope of the elastic constants versus T curves as T approaches 0 K [72]. This discontinuity can be attributed to static energy minimization predicting metastable states of strained UN supercells. Thermal motion is likely to lead the strained supercells to a global minimum of the potential energy hypersurface. For this reason, we also compute the elastic constants at 1 K. The elastic constants, moduli, and Poisson's ratio at finite temperatures are shown in Fig. 3. When calculated by the Kocevski potential, 1 K elastic constants show no significant difference from those calculated at 0 K, whereas 1 K elastic constants calculated by the Tseplyaev potential led to the disappearance of the discontinuity. All computed elastic constants were found to be independent of the amount of strain within the computational uncertainty.

In Fig. 3a, C_{12} and C_{44} computed by the Tseplyaev potential show a good agreement with experimental values at RT, whereas it overestimates RT C_{11} by more than 35%. On

Table 1: UN elastic constants (GPa) as calculated by both potentials. Experimental elastic constants are at 290 K.

	C_{11}	C_{12}	C_{44}	B
Tseplyaev potential (0 K)	586.6	110.5	54.7	269.2
Tseplyaev potential (1 K)	602.1	125.5	54.9	284.4
Kocevski potential (0 K)	425.4	117.0	71.0	219.8
Expt. [73]	423.9	98.1	75.7	206.7

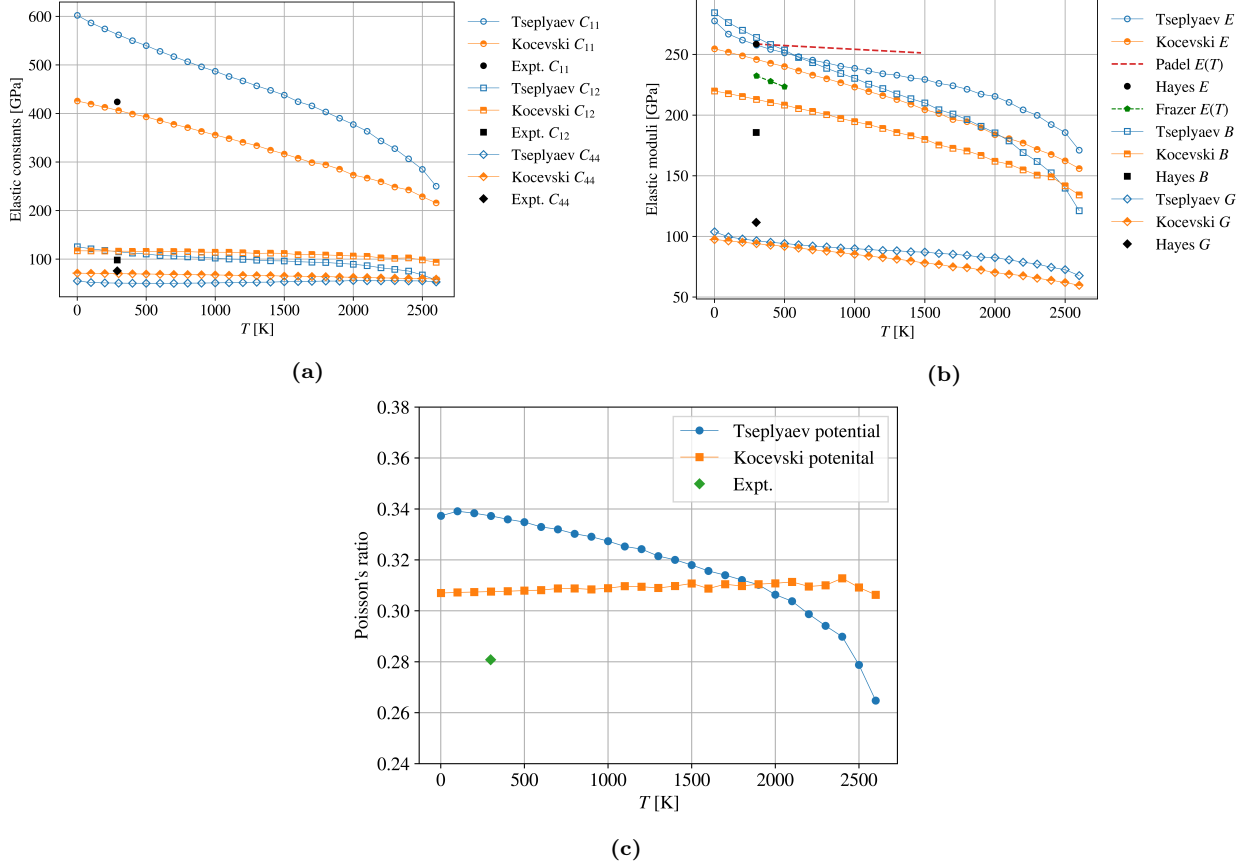


Figure 3: Computations of the temperature variation of (a) UN elastic constants, C_{11} , C_{12} , and C_{44} , (b) UN Young's modulus, E , bulk modulus, B , and shear modulus, G , and (c) Poisson's ratio as calculated by both potentials. The experimental data points in (a) are from Salleh *et al.* (1986) [73]. The experimental data points in (b) and (c) are from Hayes *et al.* (1990) [74]. The experimental variation of Young's modulus with temperature in (b) is due to Padel and de Novion [75], which Hayes *et al.* assumed to be valid also for UN's bulk and shear moduli, and due to the more recent study by Frazer *et al.* [76].

the other hand, all elastic constants calculated by the Kocevski potential agree well with the experimental values at RT. Regarding the elastic moduli (Fig. 3b), the Tseplyaev potential reproduces the experimental Young's modulus by Hayes *et al.* [74] at RT, while the RT value calculated by the Kocevski potential can be regarded as an average estimate of the value of Hayes *et al.* [74] and Frazer *et al.* [76]. The Tseplyaev potential overestimates the UN bulk modulus by more than 40%, whereas the Kocevski potential shows a better prediction and only overestimates it by about 15%. Both potentials slightly underestimate

290 the shear modulus, G . The Kocevski potential shows a good prediction of the UN Poisson's
 291 ratio compared to the experimental value at RT with an error of about 10% (Fig. 3c) and
 292 predicts a more or less constant Poisson's ratio as assumed by Hayes *et al.* [74]. However,
 293 the Tseplyaev potential overestimates the RT Poisson's ratio by about 20% and predicts a
 294 decrease of the Poisson's ratio with increasing temperature, which is related to the significant
 295 softening of the bulk modulus.

296 The only experimental measurements of the temperature variation of the UN elastic
 297 properties are the studies by Padel and de Novion [75] and by Frazer *et al.* [76] on the tem-
 298 perature dependence of UN Young's modulus. Padel and de Novion [75] report a temperature
 299 dependence of Young's modulus of the form:

$$E(T) = E_0 (1 - 2.375 \times 10^{-5}T) \quad (16)$$

300 in the temperature range of 298-1473 K, whereas Frazer *et al.* predict a dependence of the
 301 form:

$$E(T) = 245.78 - 0.0449T \quad (17)$$

302 in the temperature range of 300-500 K.

303 Eq. (16) predicts a softening rate that is much slower than that predicted by either
 304 potential as is obvious in Fig. 3b, whereas, despite its limited range, the softening rate implied
 305 by Frazer *et al.*'s data [76] seems to agree better with that predicted by both potentials. Hayes
 306 *et al.* [74] assumed the temperature dependence of Eq. (16) applies for all elastic properties
 307 except for Poisson's ratio, which they assumed to be independent of temperature. This
 308 latter assumption agrees with Poisson's ratio calculated by the Kocevski potential which
 309 can be approximated as temperature-independent. Kocevski *et al.* [27] also calculated the
 310 temperature variation of the UN elastic properties using their potential. Our results generally
 311 agree with theirs for all elastic properties except for Poisson's ratio which they estimated
 312 to be ~ 0.22 at RT compared to the experimental value of ~ 0.28 and our value of 0.31.
 313 The reason for this discrepancy is that they calculated Poisson's ratio from the formula:
 314 $\nu = C_{12}/(C_{11} + C_{12})$, which assumes the elastic constants are of an isotropic material which
 315 is not the case for UN, as $C_{11} - C_{12} \neq 2C_{44}$ [73, 77].

316 The computed Debye temperatures using different methods are given in Table 2 and
 317 compared to values reported in the literature. Values calculated in this work fall within
 318 the range 355-368 K and agree with the values measured by Adachi *et al.* [78], Scarbrough
 319 *et al.* [56], and Whaley *et al.* [79]. A large scatter is evident in the experimental Debye
 320 temperature values which range from 181-364 K. Scarbrough *et al.* [56] suspected that the
 321 values reported by Counsell *et al.* [55] and Westrum and Barber [80] (276 K and 289 K,
 322 respectively) are likely affected by the presence of magnetic specific heat. Salleh *et al.* [73]
 323 report a value of $\theta_D = 282$ K without any reference to the method they used to derive it.
 324 It's interesting to note that when Salleh *et al.*'s RT elastic constants are substituted into the
 325 Anderson and Siethoff-Ahlborn methods, they give values of $\theta_D = 365$ K and $\theta_D = 373$ K,
 326 respectively.

327 Baranov *et al.* [81] made a mistake in their estimation of the Debye temperature. They
 328 computed the Debye frequency using $\omega_D = v_0 k_D$, where v_0 is the average phonon group
 329 velocity estimated from Eq. (3) with $v_0 = 2990$ m/s (given that $v_l = 4740$ m/s and $v_t =$
 330 2691 m/s) and $k_D = (6\pi^2/\Omega)^{1/3}$, where Ω , the volume of the primitive UN unit cell, is equal

Table 2: UN Debye temperature values estimated in this work and reported in the literature.

Method	Reference	θ_D
Tseplyaev potential + Anderson method	This work	365 K
Tseplyaev potential + Siethoff-Ahlborn method	This work	356 K
Kocevski potential + Anderson method	This work	355 K
Kocevski potential + Siethoff-Ahlborn method	This work	356 K
Sound-velocity measurements in polycrystalline UN	Adachi <i>et al.</i> [78]	339 K
Sound-velocity measurements in polycrystalline UN	Whaley <i>et al.</i> [79]	361-364 K
Specific heat measurements in the temperature range 1.3-4.6 K	Scarborough <i>et al.</i> [56]	324 K
Specific heat measurements in the temperature range 5-350 K	Westrum and Barber [80]	289 K
Specific heat measurements in the temperature range 11-320 K	Counsell <i>et al.</i> [55]	276 K
Not reported	Salleh <i>et al.</i> [73]	282 K
Derived from the UN phonon spectrum measured at 4.2 K	Baranov <i>et al.</i> [81]	181 K
DFT calculation	Mei <i>et al.</i> [9]	244 K

331 to $a^3/4$, a being the lattice parameter [82]. Instead of using the volume of the *primitive* UN
 332 unit cell, they used the volume of the conventional unit cell, which led to an underestimation
 333 of the Debye temperature $\theta_D = \hbar\omega_D/k_B$. Instead of $\theta_D = 181$ K, their appropriate value
 334 should have been $\theta_D = 289$ K. Interestingly, when using the formula $v_0 = (v_l + 2v_t)/3$ to
 335 average the velocities of the acoustic branches [82], $v_0 = 3373$ m/s and Baranov *et al.*'s
 336 $\theta_D = 326$ K, which is close to our calculated values. Based on this analysis, it can be
 337 concluded that the variation of the experimental Debye temperature between the two ranges
 338 276-289 K and 324-365 K can partly be attributed to the differences in the averaging formulas
 339 used to estimate the average acoustic phonon group velocity. Another contribution is the
 340 antiferromagnetic nature of UN which leads the θ_D estimated from specific heat data to
 341 be smaller than that estimated from elastic constants as pointed out by Whaley *et al.* [79].
 342 Based on this analysis, we can conclude that the average UN θ_D is around 362 K as estimated
 343 from both experimental and computed elastic constants.

344 3.4. Specific heat capacity

345 UN C_P and its components are shown in Fig. 4. C_{exp} (Fig. 4c) is calculated from functions
 346 fitted to the UN LTEC (Eqs. (B.1) and (B.2)) and bulk modulus (Eqs. (B.3) and (B.4)), and
 347 C_{anharm} (Fig. 4d) is calculated from functions fitted to the values of C_P (Eqs. (B.5) and (B.6))
 348 and C_V (Eqs. (B.7) and (B.8)) calculated by both potentials. It can be seen in Fig. 4a that
 349 the Tseplyaev potential compares well with the UN C_P experimental correlation from Hayes
 350 *et al.* [33]. However, care must be taken when comparing to the high-temperature values of
 351 this correlation as discussed by Galvin *et al.* [71]. Both potentials agree in the computed C_P
 352 and C_V up to about 1200 K and 700 K, respectively, whereas at higher temperatures, the
 353 Kocevski potential significantly underestimates both C_P and C_V . The Tseplyaev potential
 354 predicts that the anharmonic contribution is nearly zero at low and intermediate tempera-
 355 tures, and only becomes significant at $T > 1800$ K, whereas the Kocevski potential predicts
 356 a minor contribution across the entire temperature spectrum. As can be seen in Fig. 4,
 357 the discrepancy between the C_P computed by both potentials (~ 30 J/mol-K at 2500 K)
 358 can almost completely be attributed to a difference in the computed C_V (~ 10 J/mol-K at
 359 2500 K) and a difference in the estimated C_{anharm} (~ 20 J/mol-K at 2500 K), whereas the
 360 difference in the thermal expansion contribution is quite small (~ 1 J/mol-K at 2500 K). It is

interesting to note that the structural inaccuracies of the Tseplyaev potential in determining both the bulk modulus and the LTEC nearly balance and cancel out giving a C_{exp} value that is very close to that predicted by the Kocevski potential at low temperatures. That is, the Tseplyaev-potential predictions of UN properties are energetically accurate despite the observed structural and elastic inaccuracies.

C_V and C_{anharm} are completely determined by the phonon properties of the material, and, thus, to understand why the Kocevski potential underestimates the UN C_P , a deeper investigation of the UN phonon properties as predicted by both potentials is necessary and will be shown in [Section 3.5](#).

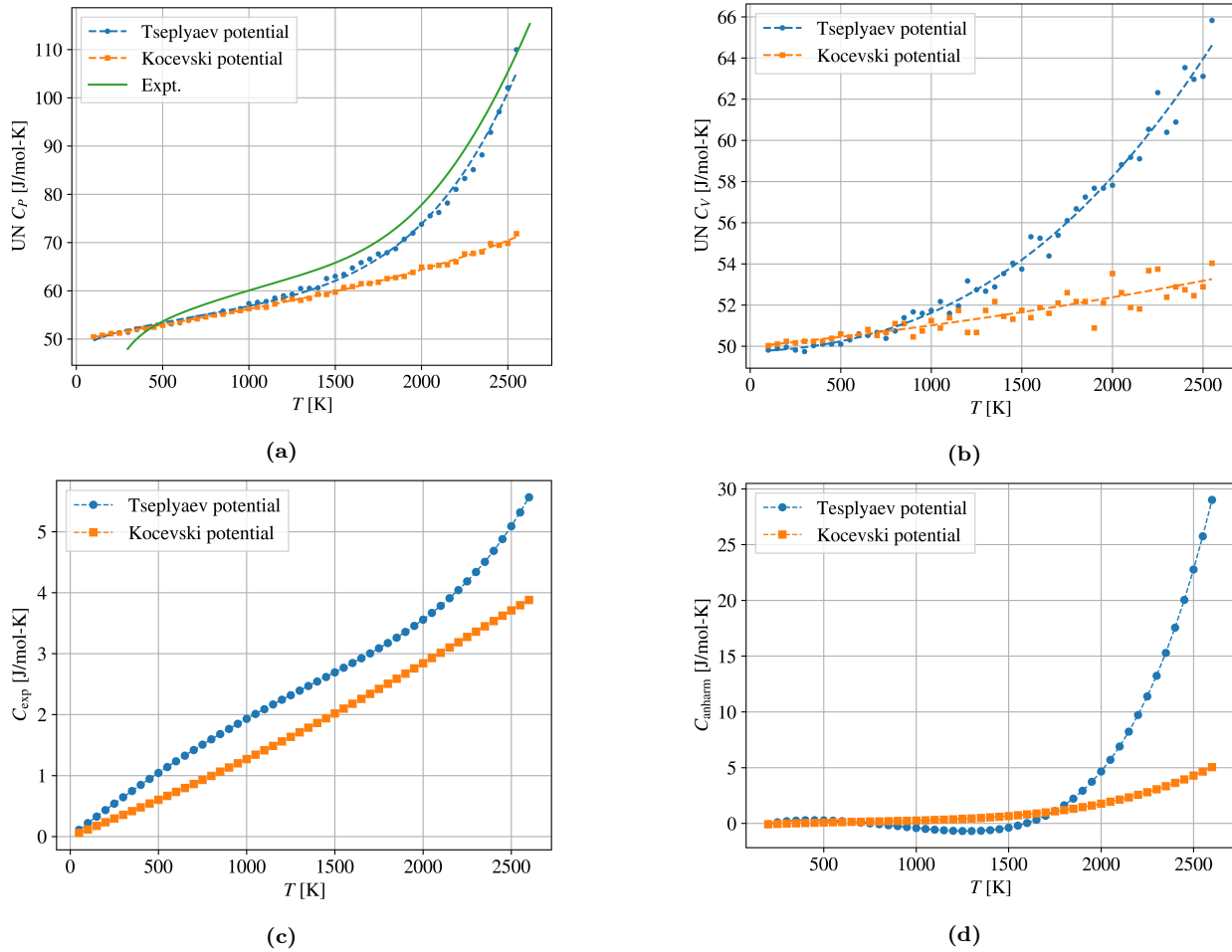


Figure 4: (a) C_P and (b) C_V of UN as calculated by both potentials and compared to the empirical correlation of Hayes *et al.* (1990) [33]. (c) The thermal expansion contribution to the specific heat. (d) The anharmonic non-expansive contribution to the specific heat.

3.5. Phonon properties

The results for the UN phonon properties are shown in [Fig. 5](#). Experimental data for UN phonon band structure and density of states (DOS) were measured by Jackman *et al.* [83] and Aczel *et al.* [84] at temperatures of 4.2 K and 5 K, respectively. Given that anharmonicity should be negligible at these cryogenic temperatures, we have carried out

phonon calculations in the harmonic approximation for comparison. It can be observed from the phonon band structure (Fig. 5a) and phonon DOS (Fig. 5b) that both potentials show a good qualitative agreement with the experimentally observed acoustic phonon spectrum while overestimating the acoustic phonon DOS. It can also be seen in Fig. 5a that the Tseplyaev potential only predicts the upper portion of the optical phonon spectrum with moderate qualitative agreement, whereas it completely misses the lower optical branches. Fig. 5b shows that the optical phonon frequency range predicted by the Kocevski potential is overestimated by about 1.9 THz compared to experimental measurements, incorrectly describing all optical branches.

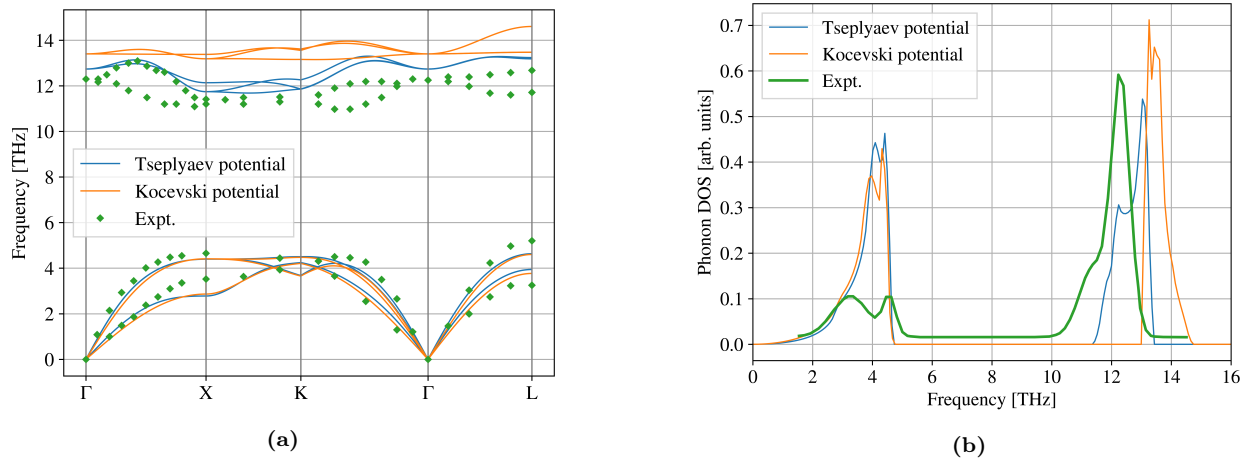


Figure 5: (a) UN phonon band structure as calculated by both potentials and compared to the experimental data of Jackman *et al.* [83]. (b) UN phonon density of states (DOS) as calculated by both potentials and compared to the inelastic neutron scattering data of Aczel *et al.* [84]. The areas under the phonon DOS plots have been normalized to 1 to allow comparison between calculations and the experiment.

The acoustic phonon spectrum and low-frequency DOS are related to the vibrations of the heavier uranium atoms, whereas the optical phonon spectrum and high-frequency DOS are related to the vibrations of the lighter nitrogen atoms [81, 45]. Therefore, it can be concluded that both potentials accurately model the uranium atom vibrations whereas only the Tseplyaev potential can qualitatively model the nitrogen atom vibrations. From these results, the Kocevski potential underestimation of the UN C_P compared to that predicted by the Tseplyaev potential can be attributed to the Kocevski potential overestimation of the optical phonon frequency range. The contribution of the optical phonons to the specific heat can be treated by the Einstein model. Due to their nearly flat dispersion curve, optical phonons are approximated within the Einstein model as having a single average frequency, ω_E , independent of k . From the experimental UN dispersion curve, $\omega_E = 12.0$ THz, whereas $\omega_E = 12.5$ THz for the Tseplyaev potential, and $\omega_E = 13.9$ THz for the Kocevski potential. Because phonons are bosons, they follow the Bose-Einstein distribution [45]:

$$f_{BE} = \frac{1}{\exp(\hbar\omega/k_B T) - 1} \quad (18)$$

where f_{BE} quantifies the mean number of phonons of frequency ω present in thermal equilibrium at temperature T [85]. With the Kocevski potential overestimating ω_E , it predicts

399 a smaller average number of excited optical phonons, which leads to a smaller contribution
400 of the optical phonons to the UN specific heat. Torres *et al.* [59] also observed the same
401 trend while analyzing the phonon properties predicted by existing UO_2 empirical potentials.
402 By including both harmonic and higher-order force constants in their phonon calculations,
403 they found that UO_2 empirical potentials that overestimate the 0 K optical phonon frequency
404 range tend to underestimate the specific heat, especially at near-melting temperatures. Zhou
405 *et al.* [86] also made a similar observation about the Stillinger-Weber potential of GaN, and
406 attributed its underestimation of the specific heat at high temperatures to the overestimated
407 optical phonon range. The Debye temperature quantifies the temperature above which all
408 phonon modes become excited and below which some phonon modes freeze out [85]. Based
409 on our analysis in Section 3.3, θ_D is around 362 K, which means that even at temperatures
410 near RT we can expect optical phonons to contribute to the UN specific heat. Baranov *et al.*
411 [81] also noted that due to the ionic character of the UN chemical bond, optical phonons are
412 expected to predominate the oscillation spectrum of the UN lattice at temperatures above
413 θ_D .

414 The agreement between the lattice thermal conductivity predicted by Galvin *et al.* [71]
415 using both potentials despite the discrepancy of the predicted specific heats can be under-
416 stood if we note that the two potentials predict the same acoustic phonon spectrum and DOS
417 at 0 K. For bulk materials, the thermal conductivity is largely dictated by acoustic phonons
418 because they are the main heat carriers [87]. In contrast, the contribution of optical phonons
419 to the thermal conductivity of bulk materials is very small due to their short lifetimes and
420 low group velocities [88].

421 3.6. Point defect formation energies

422 Perfect $6 \times 6 \times 6$ supercells of UN were energy-minimized at 0 K using the conjugate
423 gradient algorithm implemented in LAMMPS. A fractional energy tolerance of 1×10^{-9} was
424 used allowing volume change. For the Tseplyaev potential, we used energy tolerances in the
425 range 10^{-6} - 10^{-15} and found that the raw formation energies of the defective supercells vary by
426 several eV with decreasing the energy tolerance down to a tolerance of 10^{-9} at which the raw
427 formation energy becomes somewhat insensitive to the energy tolerance. This is indicative
428 of the complex potential energy surface predicted by the Tseplyaev potential and the likely
429 existence of several metastable states. This strong dependence of the raw formation energy
430 on energy tolerance was not observed for the Kocevski potential. The cohesive energies
431 of UN, α -U, and UN_2 and chemical potentials were calculated for both potentials and are
432 shown in Tables B.7 and B.8. It should be noted that the Kocevski potential predicts
433 positive cohesive energy for α -U (i.e., it cannot predict a stable α -U phase), which would
434 lead to unphysical chemical potentials and incorrect formation energies for the U-rich and
435 stoichiometric conditions. For this reason, point defects under U-rich and stoichiometric
436 conditions are not considered for the Kocevski potential in this work.

437 For the 0 K calculations, point defects were then introduced into $6 \times 6 \times 6$ UN supercells.
438 U and N interstitials were inserted only in cubic interstitial sites. Yang and Kaltsoyannis
439 [19] have observed that when a U Frenkel defect is introduced within a UN supercell, it is
440 annihilated by the tiny atomic movements of the relaxation process. To prevent this phe-
441 nomenon, the initial forces on all inserted interstitials were set to zero. Defective supercells
442 were relaxed using the same procedure used for the perfect supercells.

To avoid the possibility of defective supercells converging to metastable energy states by static minimization at 0 K, the 0 K formation energies are averaged over many defect configurations, and, additionally, the formation energies are also calculated at 1 K. $8 \times 8 \times 8$ supercells of UN are equilibrated in the *NPT* ensemble for 50 ps, where the system's potential energy is averaged over the last 20 ps. Point defects are inserted in the equilibrated UN supercells, and the defective system is allowed to evolve under the *NPT* ensemble for 50 ps where the system's potential energy is also averaged over the last 20 ps. The calculation is repeated using five unique initial velocity distributions, utilizing the average potential energy of this sample to obtain defect energetics. Chemical potentials and formation energies are calculated using the same procedure employed at 0 K. The Tseplyaev potential is also used to calculate the finite-temperature formation enthalpy for U FD, N FD, and SD with 15 unique initial velocity distributions in the temperature range of 100-1500 K. The 1500 K limit is chosen because in UN diffusion begins to be experimentally observed at this temperature [89]. Thus, at and beyond 1500 K, the measured raw formation enthalpies would be affected by defect migration.

Table 3: Formation energies (eV) for stoichiometric point defects. FD stands for Frenkel defect, and SD stands for Schottky defect. A semi-bound SD is composed of two vacancies at (0, 0, 0) and (0.5, 0.5, 0.5).

	Tseplyaev potential		Kocevski potential		DFT
	0 K	1 K	0 K	1 K	
Unbound U FD	9.32	8.02	14.41	14.30	9.46 [19], 6.31-10.19 [10]
Bound U FD	7.26	-	10.3	-	-
Unbound N FD	4.67	4.50	4.03	4.00	4.90-5.04 [19], 4.43-4.95 [10]
Bound N FD	3.76	-	3.23	-	-
Unbound SD	4.57	4.52	3.98	3.88	4.96-5.15 [19], 4.25-5.47 [10]
Semi-bound SD	4.51	-	3.99	-	-
Bound SD (divacancy)	4.35	-	3.04	-	4.17 [19]

Table 4: Formation energies (eV) for non-stoichiometric point defects. Standard Kröger-Vink notation [90] has been used for point defects but with charges omitted due to the inability of MD to simulate charged defects.

	U-rich		Stoichiometric		N-rich						
	Tseplyaev 0 K	1 K	DFT	Tseplyaev 0 K	1 K	DFT	Tseplyaev 0 K	1 K	Kocevski 0 K	1 K	DFT
V _U	3.45	3.33	3.17-3.43 [19], 3.27-3.86 [10]	2.19	2.14	2.75-3.01 [19]	0.93	0.95	0.60	0.54	2.34-2.60 [19], 2.09-2.58 [10]
V _N	1.11	1.29	1.76-1.90 [19], 0.62-1.86 [10]	2.37	2.48	2.18-2.31 [19]	3.62	3.67	3.35	3.34	2.59-2.72 [19], 1.42-2.82 [10]
U _i	6.43	3.99	2.81-6.33 [10]	7.69	5.18	-	8.95	6.37	13.82	13.76	3.79-7.78 [10]
N _i	3.73	3.21	2.96-3.82 [10]	2.47	2.02	-	1.21	0.83	0.89	0.66	2.00-3.01 [10]
U _N	1.61	1.86	1.74-3.16 [10]	4.13	4.24	-	6.65	6.62	18.32	15.90	3.72-5.52 [10]
N _U	9.32	5.84	5.99-7.67 [10]	6.80	3.46	-	4.28	1.08	4.71	1.70	4.06-5.19 [10]

The calculated formation energies are reported in Tables 3 and 4. Bound SD and FD are formed by introducing the two vacancies, and the vacancy and interstitial, respectively, within the same unit cell, whereas unbound SD and FD are formed by introducing the two vacancies, and the vacancy and interstitial, respectively, within different unit cells. Dashes in Table 3 for bound defects at 1 K indicate that these defects relaxed to the defect-free crystal structure. The formation energy of the N FD is slightly higher than the formation energies of the unbound SD and divacancy due to the lattice's compact structure which offers limited room for an interstitial. The formation energies predicted by the Tseplyaev potential at 0 K and 1 K are generally consistent with each other except for the values predicted for unbound

467 U FD, U_i , and N_U which show differences in the range 1.30-3.48 eV, with the 0 K values being
 468 generally larger than the 1 K values. This is because calculating the formation energies at 1
 469 K using the Tseplyaev potential allows us to approach the ground state of the defect struc-
 470 ture, whereas the calculation at 0 K fails to do so. This is especially true for U_i , whose most
 471 stable configuration in UN is reported as the dumbbell configuration [24], whereas, by visual
 472 inspection of the U_i structure at 0 K (not shown), U_i still resides at the cubic interstitial
 473 site after static minimization using the Tseplyaev potential. The difference in U_i formation
 474 energy between 0 K and 1 K also explains the difference in the formation energy of U FD.
 475 This discrepancy most likely signifies that the Tseplyaev potential predicts metastable states
 476 for the defected UN supercells at 0 K, a situation that we also encountered with strained
 477 UN supercells at 0 K. Thus, caution should be exercised when utilizing or examining 0 K
 478 defect properties calculated by the Tseplyaev potential. The formation energies predicted by
 479 the Tseplyaev potential generally show excellent agreement with the DFT-predicted values
 480 for U-rich, N-rich, and stoichiometric conditions. The Kocevski potential predicts formation
 481 energies for N FD and SD in agreement with DFT, but it overestimates the U FD defect by
 482 more than 4 eV. As explained previously, the Kocevski potential cannot predict formation
 483 energies for U-rich and stoichiometric conditions due to the inability to describe metallic
 484 U. However, for N-rich conditions, the formation energies predicted by the Kocevski poten-
 485 tial qualitatively agree with DFT-values for most defects except for U_i and U_N , which are
 486 overestimated by a factor of 2-3. It can be concluded that the Tseplyaev potential shows a
 487 better performance in the calculation of point defect formation energy, whereas the Kocevski
 488 potential is only suitable for stoichiometric point defects. It can also be concluded that, in
 489 UN, hypo-stoichiometry is accommodated by V_N and U_N , whereas hyper-stoichiometry is
 490 accommodated by V_U and N_i .

491 Lastly, it is interesting to note that the formation energy of U_N at 1 K is nearly one-half
 492 of its value at 0 K for all cases. Based on visual inspection it was noticed that the following
 493 reaction takes place:



494 where $NN-D\langle 111 \rangle$ refers to the N-N dumbbell along the $\langle 111 \rangle$ direction. This reaction likely
 495 leads to a reduction in the formation energy. Although Kuksin *et al.* [24] did not consider N_U
 496 they reported similar reactions for other defect types in UN as well as uranium monocarbide
 497 (UC).

498 Formation enthalpies of U FD, N FD, and SD in UN as a function of temperature are
 499 shown in Fig. 6. As expected, the standard deviation increases with increasing temperature.
 500 The average formation enthalpy of U FD is confined to about 7-8 eV, whereas those of N
 501 FD and SD are confined to about 4-5 eV, with no apparent dependence on temperature.

502 3.7. UN_2 , α - U_2N_3 and β - U_2N_3

503 3.7.1. Thermophysical properties

504 The UN_2 lattice parameter and C_P predicted by both potentials are shown in Figs. 7a
 505 and 7b, respectively. The Tseplyaev potential gives a better prediction of the UN_2 lattice
 506 parameter with a slight underestimation and predicts a phase transition at about 800 K. On
 507 the other hand, the Kocevski potential overestimates the UN_2 lattice parameter and predicts
 508 a stable UN_2 crystal structure up to 1400 K. It should be noted that the phase transition

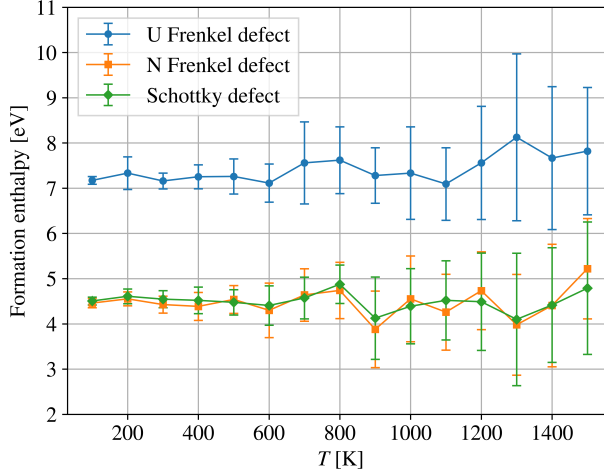


Figure 6: Defect formation enthalpy as a function of temperature for the unbound U Frenkel defect, unbound N Frenkel defect, and unbound Schottky defect in UN as a function of temperature as calculated by the Tseplyaev potential. Error bars correspond to one standard deviation.

temperature of UN_2 is 1324–1405 K [4, 38]. It is also worth mentioning that Silva *et al.* [31] reported lattice constants of UN_2 and $\alpha\text{-U}_2\text{N}_3$ as a function of temperature; however, their samples were not of high purity but rather included the $\text{UN}_2/\alpha\text{-U}_2\text{N}_3$ solid solution, and, thus, are not ideal for comparison. The Tseplyaev potential overestimates the $\text{UN}_2 C_P$ compared to that calculated by the Kocevski potential, a trend that was also observed for UN. Due to the lack of experimental measurements, we compare the predicted C_P with the Dulong–Petit value which, for a compound, is defined as $3nR$, n being the number of atoms per formula unit ($n = 3$ for UN_2 , and $n = 5$ for α - and $\beta\text{-U}_2\text{N}_3$), and R being the gas constant [91]. The Dulong–Petit value serves as a theoretical lower limit on C_P data for solids well above room temperature and is useful to compare against in the absence of experimental measurements. The $\text{UN}_2 C_P$ predicted by both potentials approach the Dulong–Petit value around room temperature and deviate from it at higher temperatures, which is the theoretically expected trend [85]. In general, the specific heat reaches the Dulong–Petit value at temperatures near and below room temperature because of the inability of MD simulations to model the quantum effects that would otherwise lead to the decrease of specific heat with temperature up to 0 K according to the Debye model [85]. Thus, the classical thermodynamic Dulong–Petit value holds at low temperatures. However, at high temperatures, the specific heat is swamped by phonon dynamics which can be modeled by MD to some level of accuracy.

The Tseplyaev potential could not predict a stable crystal structure above 0 K for either $\alpha\text{-U}_2\text{N}_3$ or $\beta\text{-U}_2\text{N}_3$, so we only discuss the finite temperature α - and $\beta\text{-U}_2\text{N}_3$ properties predicted by the Kocevski potential (Fig. B.11). The Kocevski potential predicts that the $\alpha\text{-U}_2\text{N}_3$ phase has a stable crystal structure up to about 1000 K. For $\alpha\text{-U}_2\text{N}_3$, the Kocevski potential overestimates the lattice parameter, and for $\beta\text{-U}_2\text{N}_3$, it overestimates the a parameter and underestimates the c parameter. The α - and $\beta\text{-U}_2\text{N}_3 C_P$ predicted by the Kocevski potential nearly coincide and approach the Dulong–Petit value around RT. Additionally, the Kocevski potential predicts that the $\beta\text{-U}_2\text{N}_3$ crystal structure can be stabilized at very low

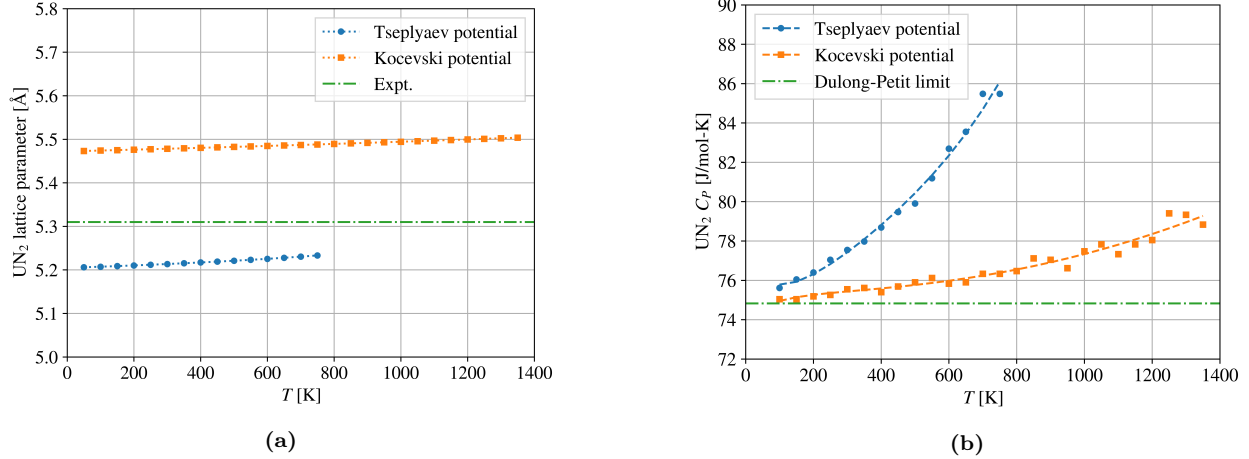


Figure 7: (a) The lattice parameter of UN_2 calculated by both potentials as a function of temperature. (b) $\text{UN}_2 C_P$ calculated by both potentials as a function of temperature. C_P calculated by the Tseplyaev and Kocevski potentials are fitted to Eqs. (B.9) and (B.10), respectively. The experimental lattice parameter of UN_2 is taken from Lu *et al.* [92] and included as a horizontal line because the temperature at which it was measured is not reported.

temperatures.

As mentioned earlier, the Tseplyaev potential is a modified version of the ADP developed by Kuskin *et al.* [24]. The authors reported that Kuksin's potential could stabilize the crystal structures of α - and β - U_2N_3 . However, Tseplyaev and Starikov [25] don't report any capability of the modified version of the potential to simulate polymorphs of U_2N_3 at zero pressure. Thus, it appears that in the modification of the potential to improve UN property prediction, the capability was lost for other phases in the U-N system.

3.7.2. Elastic properties

The 0 K elastic constants of UN_2 are shown in Table 5. The predictions of the Kocevski potential show a good agreement with the DFT predictions for C_{12} and C_{44} , whereas it underestimates C_{11} by about 40%. The predictions of the Tseplyaev potential show much larger errors: it overestimates C_{11} and C_{12} by more than 70%, and 40%, respectively, and its C_{44} value is overestimated by nearly a factor of 5. The temperature dependence of the UN_2 elastic constants and moduli are shown in Fig. 8. The Kocevski potential shows general qualitative agreement with the UN_2 elastic moduli predicted by DFT, whereas the Tseplyaev potential greatly overestimates all elastic moduli and fails to give qualitative predictions. The Kocevski potential shows minimal softening of the UN_2 elastic properties with increasing temperature.

Table 5: UN_2 elastic constants (GPa) at 0 K as calculated by both potentials. The DFT values are from Lu *et al.* [92] and have been calculated using the GGA+ U approach with $U = 2$ eV.

	C_{11}	C_{12}	C_{44}
Tseplyaev potential	856.2	201.4	291.7
Kocevski potential	275.9	184.1	67.8
DFT [92]	488.2	140.5	55.3

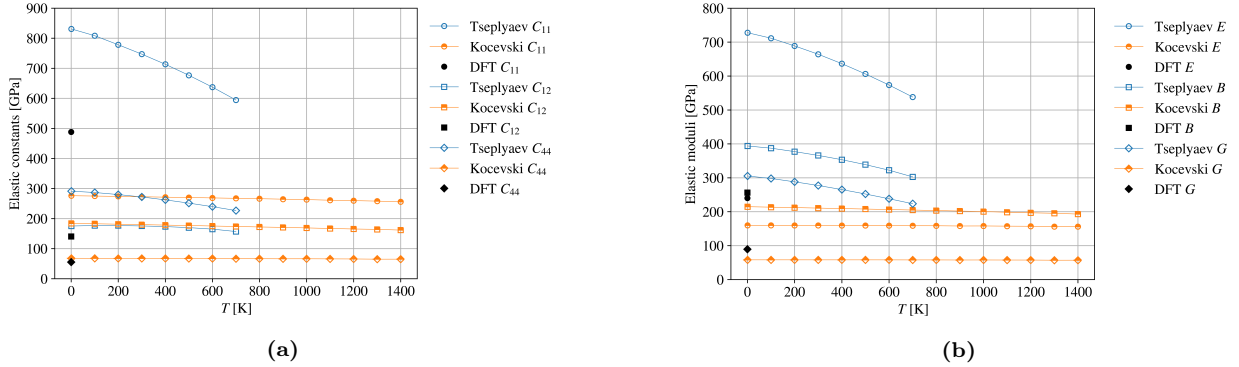


Figure 8: The predicted temperature variation of (a) UN₂ elastic constants, C_{11} , C_{12} , and C_{44} , (b) UN₂ Young's modulus, E , bulk modulus, B , and shear modulus, G . The DFT values are from Lu *et al.* [92].

The 0 K elastic constants of α -U₂N₃ calculated by the Kocevski potential are $C_{11} = 185.4$ GPa, $C_{22} = 141.8$ GPa, and $C_{44} = 41.8$ GPa, whereas the elastic constants and moduli calculated at finite temperatures are shown in Figs. 9a and 9b, respectively. To the best of our knowledge, no experimental or DFT elastic property data exist for α -U₂N₃. It can be observed that α -U₂N₃ is generally softer than UN₂ which is expected because, as explained earlier, the α -U₂N₃ conventional unit cell lacks 16 N atoms, and thus has fewer bonds compared to the $2 \times 2 \times 2$ UN₂ supercell.

For β -U₂N₃, the 0 K elastic constants are shown in Table 6. The predictions of both potentials satisfy the elastic stability criteria of the hexagonal lattice and nearly agree, except for C_{33} which the Tseplyaev potential overpredicts by a factor of 23, and C_{44} which the Tseplyaev potential underestimates with an error of about 50%—all relative to the values predicted by the Kocevski potential at 0 K. The bulk modulus predicted by the Kocevski potential agrees perfectly with that predicted by the DFT study of Lu *et al.* [92]. The elastic constants and bulk modulus of β -U₂N₃ predicted by the Tseplyaev potential vary significantly by varying the strain, whereas those predicted by the Kocevski potential show a negligible dependence on the strain value. This is indicative of potential instabilities using the Tseplyaev potential for β -U₂N₃, which are confirmed through the evaluation of the structure at finite temperatures, which decomposes as discussed. The variation of the β -U₂N₃ elastic constants with temperature is shown in Fig. 10a. C_{11} and C_{33} show observable softening, C_{12} shows a slower softening rate, and C_{13} and C_{44} are nearly constant. β -U₂N₃ elastic moduli are shown in Fig. 10b. As explained earlier, the predicted bulk modulus qualitatively agrees with DFT values. In general, further experimental investigations are required to validate the predicted properties of UN₂, α -U₂N₃, and β -U₂N₃.

Table 6: β -U₂N₃ elastic properties (GPa) as calculated by both potentials. $B = 232$ GPa has been calculated by Evarestov *et al.* [7] using the LCAO DFT approach. $B = 209.2$ GPa has been calculated by Lu *et al.* [92] using the GGA+ U approach with $U = 2$ eV.

	C_{11}	C_{12}	C_{13}	C_{33}	C_{44}	B
Tseplyaev potential	372.4	166.8	118.1	5680.1	30.0	534.5
Kocevski potential	357.0	224.2	140.7	242.7	64.5	210.0
DFT						232 [7], 209.2 [92]

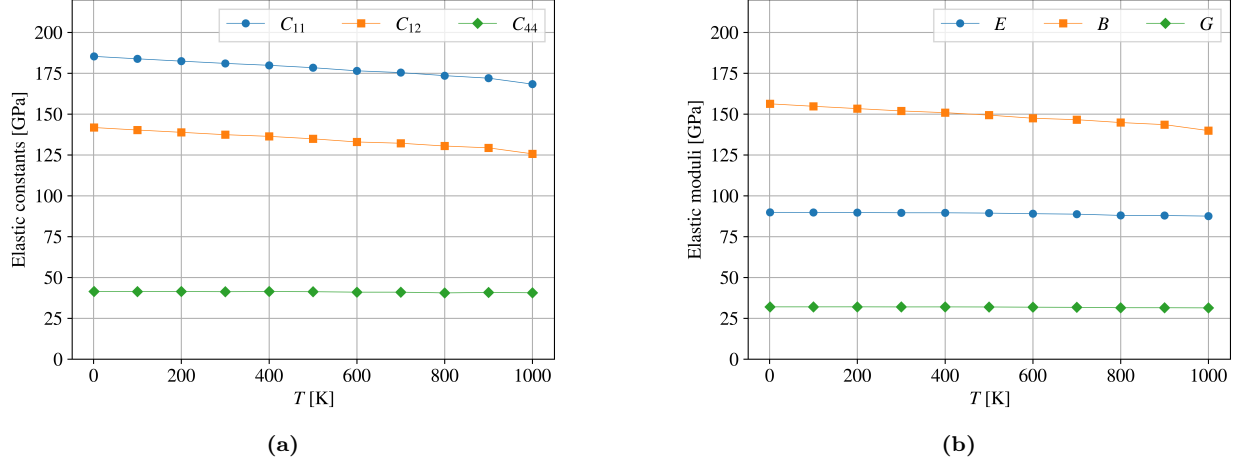


Figure 9: (a) Elastic constants, C_{11} , C_{12} , and C_{44} , (b) Young’s modulus, E , bulk modulus, B , and shear modulus, G , of $\alpha\text{-U}_2\text{N}_3$ as calculated by the Kocevski potential.

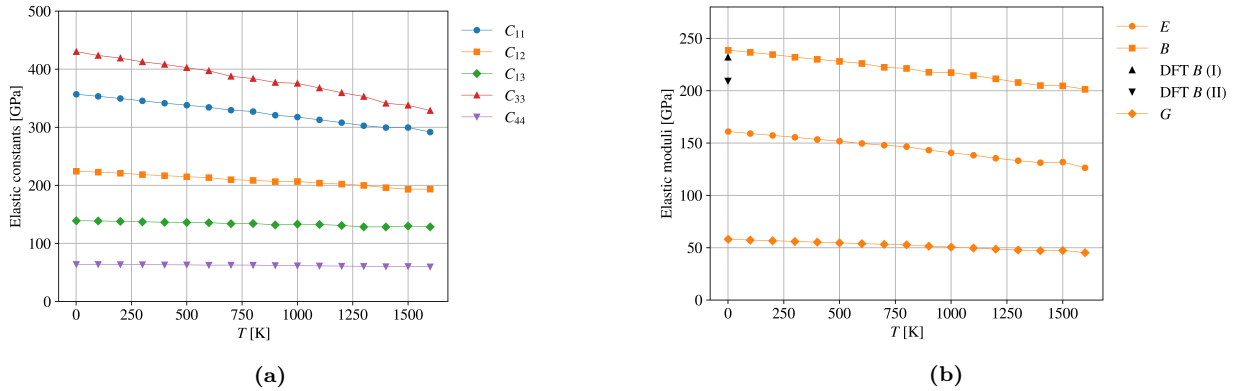


Figure 10: (a) Elastic constants, C_{11} , C_{12} , C_{13} , C_{33} , and C_{44} , (b) Young’s modulus, E , bulk modulus, B , and shear modulus, G , of $\beta\text{-U}_2\text{N}_3$ as calculated by the Kocevski potential. DFT B (I) is from Evarestov *et al.* [7] and DFT B (II) is from Lu *et al.* [92].

577 4. Discussion

578 Based on the presented results, we can identify several features of both potentials. In
 579 general, the Kocevski potential shows better predictability of the structural aspects of UN,
 580 e.g., lattice parameter and elastic properties as a function of temperature, whereas the
 581 Tseplyaev potential better predicts the UN energetic aspects, e.g., the specific heat and
 582 defect formation energies. One drawback of the Kocevski potential is the overestimation
 583 of the UN optical phonon range, leading to its underestimation of the UN C_P , compared
 584 to the Hayes *et al.* [33] correlation, at temperatures greater than 1200 K. Moreover, the
 585 Kocevski potential cannot predict a stable metallic $\alpha\text{-U}$ structure. Therefore, its applicability
 586 to studies related to UN non-stoichiometry is limited. The Tseplyaev potential does an
 587 inferior job of predicting the UN elastic properties and underpredicts the experimental lattice
 588 parameter values compared to the Kocevski potential. The Tseplyaev potential predicts
 589 the UN phonon band structure with reasonable accuracy, which makes it preferable in the
 590 evaluation of thermal conductivities. Another important feature of the Tseplyaev potential is

591 that it predicts metastable states for defected UN supercells at 0 K, and thus we recommend
592 avoiding its usage at 0 K. Thus, each potential has realms of applicability for the description
593 of the UN system, and the noted drawbacks must be acknowledged when deciding which
594 potential to utilize.

595 The predictions of UN_2 properties by the Kocevski potential show better qualitative
596 agreement with the limited experimental and DFT values; however, neither potential pro-
597 duces results with a satisfactory level of accuracy. The Tseplyaev potential cannot predict
598 stable structures for α - and β - U_2N_3 and predicts premature phase change of both UN and
599 UN_2 . Thus, the Tseplyaev potential is not suitable for studies related to the stability of dif-
600 ferent uranium nitride phases. On the other hand, the Kocevski potential predicts stable α -
601 and β - U_2N_3 structures with reasonable lattice parameters, reasonably predicts the melting
602 point of UN and predicts a crystal structure stability range of UN_2 closer to that represented
603 by the U-N system phase diagrams. This makes the Kocevski potential the best option for
604 studies involving many uranium nitride phases, although more experimental data are needed
605 to further assess its predictions of UN_2 , and α - and β - U_2N_3 properties.

606 Areas of importance that have not been assessed in this study include the dynamical pro-
607 cesses of plastic deformation, i.e., dislocation formation and slip, interfacial properties, and
608 radiation damage. Such analyses are beyond the scope of this work, but potential compari-
609 son and validation should be conducted before utilization of either potential to explore these
610 phenomena. Another interesting aspect worth exploring in future studies is the high-pressure
611 phase transition that UN undergoes from the cubic $Fm\bar{3}m$ structure to the rhombohedral
612 $R\bar{3}m$ structure [93, 94, 9]. Experimentally, this transition was observed to occur at 29 GPa
613 [93], and the Tseplyaev potential predicted it to take place at a pressure of 35 GPa [25].
614 However, the Kocevski potential was never used to study this aspect.

615 5. Conclusions

616 This work aimed to evaluate two UN interatomic potentials: Tseplyaev and Starikov's
617 ADP [25] and Kocevski *et al.*'s EAM potential [27]. The study involved assessing the predic-
618 tive capabilities of these potentials for various thermophysical and elastic properties of UN,
619 UN_2 , and α - and β - U_2N_3 . The Kocevski potential underestimates the UN specific heat which
620 is attributed to its overestimation of the UN optical phonon frequency range. In terms of per-
621 formance, the Tseplyaev potential excels in capturing the energetic aspects of UN, whereas
622 the Kocevski potential performs better in modeling the UN's structural properties. Regard-
623 ing the crystal structure stability of phases, the Kocevski potential demonstrates superior
624 predictive capabilities, in that it can reasonably estimate the UN melting point and predicts
625 stable α - and β - U_2N_3 structures. In contrast, the Tseplyaev potential predicts premature
626 phase changes for both UN and UN_2 and fails to stabilize either polymorph of U_2N_3 . An
627 important limitation of the Kocevski potential is its inability to predict a stable metallic U
628 phase, making it unsuitable for studies related to UN non-stoichiometry.

629 Acknowledgements

630 The authors would like to thank Antoine Claisse for the fruitful discussions. We would
631 like to acknowledge Westinghouse Electric Company for providing funding for this work.

632 This research made use of the resources of the High-Performance Computing Center at
 633 Idaho National Laboratory, which is supported by the Office of Nuclear Energy of the U.S.
 634 Department of Energy and the Nuclear Science User Facilities under Contract No. DE-
 635 AC07-05ID14517. Mohamed AbdulHameed dedicates this work to the memory of Abu Bakr
 636 Etman.

637 Appendix A. Voigt-Reuss-Hill elastic moduli

638 For an isotropic polycrystalline material with a cubic crystal structure, the form of the
 639 VRH elastic moduli is [46, 95]:

$$B = B_V = B_R = \frac{C_{11} + 2C_{12}}{3} \quad (\text{A.1})$$

$$G_V = \frac{C_{11} - C_{12} + 3C_{44}}{5} \quad (\text{A.2})$$

$$G_R = \frac{5C_{44}(C_{11} - C_{12})}{4C_{44} + 3(C_{11} - C_{12})} \quad (\text{A.3})$$

$$G = \frac{G_V + G_R}{2} \quad (\text{A.4})$$

$$E = \frac{9BG}{3B + G} \quad (\text{A.5})$$

$$\nu = \frac{3B - 2G}{6B + 2G} \quad (\text{A.6})$$

640 For the $\beta\text{-U}_2\text{N}_3$ hexagonal crystal, the Voigt and Reuss limits on the bulk and shear
 641 moduli are formulated in terms of the components of both the stiffness tensor, C_{ij} , and the
 642 compliance tensor, S_{ij} [46, 96]:

$$B_V = \frac{2C_{11} + 2C_{12} + 4C_{13} + C_{33}}{9} \quad (\text{A.7})$$

$$B_R = \frac{1}{2S_{11} + 2S_{12} + 4S_{13} + S_{33}} \quad (\text{A.8})$$

$$B = \frac{B_V + B_R}{2} \quad (\text{A.9})$$

$$G_V = \frac{2C_{11} - C_{12} - 2C_{13} + C_{33} + 6C_{44} + 3C_{66}}{15} \quad (\text{A.10})$$

$$G_R = \frac{15}{8S_{11} - 4S_{12} - 8S_{13} + 4S_{33} + 6S_{44} + 3S_{66}} \quad (\text{A.11})$$

647 where S_{11} , S_{12} , S_{13} , S_{33} , and S_{44} are the independent components of the compliance tensor,
 648 and:

$$S_{11} = \frac{C_{11}C_{33} - C_{13}^2}{C_{11}(C_{11}C_{33} - 2C_{13}^2) - C_{12}(C_{12}C_{33} + 2C_{13}^2)} \quad (\text{A.12})$$

649

$$S_{12} = \frac{-C_{12}C_{33} + C_{13}^2}{C_{11}(C_{11}C_{33} - 2C_{13}^2) - C_{12}(C_{12}C_{33} + 2C_{13}^2)} \quad (\text{A.13})$$

650

$$S_{13} = \frac{-C_{13}}{C_{33}(C_{11} + C_{12}) - 2C_{13}^2} \quad (\text{A.14})$$

651

$$S_{33} = \frac{C_{11} + C_{12}}{C_{33}(C_{11} + C_{12}) - 2C_{13}^2} \quad (\text{A.15})$$

652

$$S_{44} = \frac{1}{C_{44}} \quad (\text{A.16})$$

653

$$C_{66} = \frac{C_{11} - C_{12}}{2} \quad (\text{A.17})$$

654

$$S_{66} = 2(S_{11} - S_{12}) \quad (\text{A.18})$$

655 **Appendix B. Supplementary information**

656 In all equations presented in this appendix, the superscript T refers to the Tseplyaev
657 potential and the superscript K refers to the Kocevski potential.

658 The temperature variation of the LTEC computed by both potentials is fitted to the
659 following functions:

660

$$\alpha_L^T = 7.321 \times 10^{-6} - 3.063 \times 10^{-11}T + 2.154 \times 10^{23}T^5 \quad (R^2 = 99.8\%) \quad (\text{B.1})$$

661

$$\alpha_L^K = 5.773 \times 10^{-6} + 3.866 \times 10^{-10}T + 1.813 \times 10^{-13}T^2 \quad (R^2 = 99.9\%) \quad (\text{B.2})$$

662 in the temperature range 50-2500 K.

663 The temperature dependence of the bulk modulus computed by both potentials is fitted
to the following quadratic functions:

664

$$B^T = 275.063 - 3.314 \times 10^{-2}T - 7.649 \times 10^{-6}T^2 \quad (R^2 = 98.4\%) \quad (\text{B.3})$$

665

$$B^K = 219.196 - 1.955 \times 10^{-2}T - 4.517 \times 10^{-6}T^2 \quad (R^2 = 99.8\%) \quad (\text{B.4})$$

666 in the temperature range of 1-2600 K.

The UN C_P and C_V computed by both potentials have been fitted to:

667

$$C_P^T = 61.612 + 4.709 \times 10^{-3}T + 3.754 \times 10^{-16}T^5 - 19.663/T^{0.1} \quad (R^2 = 99.4\%) \quad (\text{B.5})$$

668

$$C_P^K = 50.500 + 6.193 \times 10^{-3}T + 1.272 \times 10^{-13}T^4 - 1.140/T^{0.1} \quad (R^2 = 99.7\%) \quad (\text{B.6})$$

669

$$C_V^T = 49.341 + 7.144 \times 10^{-4}T + 4.016 \times 10^{-8}T^{2.5} + 0.591/T^{0.1} \quad (R^2 = 98.8\%) \quad (\text{B.7})$$

670

$$C_V^K = 49.978 + 8.757 \times 10^{-4}T + 1.616 \times 10^{-7}T^2 \quad (R^2 = 80.8\%) \quad (\text{B.8})$$

667 The UN_2 C_P calculated by both potentials are fitted to:

$$C_P^T = 54.894 + 1.803 \times 10^{-2}T + 8.717 \times 10^{-15}T^5 + 30.248/T^{0.1} \quad (R^2 = 98.9\%) \quad (\text{B.9})$$

$$C_P^K = 82.060 - 2.445 \times 10^{-3}T + 3.199 \times 10^{-6}T^2 - 10.934/T^{0.1} \quad (R^2 = 95.1\%) \quad (\text{B.10})$$

668 whereas the $\alpha\text{-U}_2\text{N}_3$ C_P calculated by the Kocevski potential is fitted to:

$$C_P^K = 155.092 - 1.686 \times 10^{-2}T + 1.534 \times 10^{-5}T^2 - 45.235/T^{0.1} \quad (R^2 = 93.3\%) \quad (\text{B.11})$$

669 and the $\beta\text{-U}_2\text{N}_3$ C_P calculated by the Kocevski potential is fitted to:

$$C_P^K = 132.240 + 7.979 \times 10^{-4}T + 2.544 \times 10^{-6}T^2 - 11.483/T^{0.1} \quad (R^2 = 91.1\%) \quad (\text{B.12})$$

Table B.7: Cohesive energies (eV) of UN, α -U and UN_2 .

	Tseplyaev potential	Kocevski potential	Reference value
UN	-16.18	-13.02	-13.6 (Expt.) [7]
α -U	-5.23 (0 K); -5.37 (1 K)	-	-5.55 (Expt.) [97]
UN_2	-24.62	-22.18	-21.5 to -17.9 (DFT) [7]

Table B.8: U and N chemical potentials (eV) for different stoichiometric conditions.

	Tseplyaev potential			Kocevski potential
	U-rich	Stoichiometric	N-rich	N-rich
μ_U	-5.23 (0 K); -5.37 (1 K)	-6.49 (0 K); -6.56 (1 K)	-7.75	-3.86
μ_N	-10.95 (0 K); -10.81 (1 K)	-9.69 (0 K); -9.62 (1 K)	-8.43	-9.16

670 References

- 671 [1] J. K. Watkins, A. Gonzales, A. R. Wagner, E. S. Sooby, B. J. Jaques, Challenges
672 and opportunities to alloyed and composite fuel architectures to mitigate high uranium
673 density fuel oxidation: Uranium mononitride, Journal of Nuclear Materials 553 (2021).
674 [doi:10.1016/j.jnucmat.2021.153048](https://doi.org/10.1016/j.jnucmat.2021.153048).
- 675 [2] C. Ekberg, D. R. Costa, M. Hedberg, M. Jokkonen, Nitride fuel for Gen IV nuclear
676 power systems, Journal of Radioanalytical and Nuclear Chemistry 318 (2018) 1713–
677 1725. [doi:10.1007/s10967-018-6316-0](https://doi.org/10.1007/s10967-018-6316-0).
- 678 [3] J. Wallenius, Nitride fuels, Comprehensive Nuclear Materials 5 (2020) 88–101. [doi:
679 10.1016/B978-0-12-803581-8.11694-7](https://doi.org/10.1016/B978-0-12-803581-8.11694-7).
- 680 [4] M. Uno, T. Nishi, M. Takano, Thermodynamic and thermophysical properties of
681 the actinide nitrides, Comprehensive Nuclear Materials: Second Edition (2020) 202–
682 231[doi:10.1016/B978-0-12-803581-8.11749-7](https://doi.org/10.1016/B978-0-12-803581-8.11749-7).

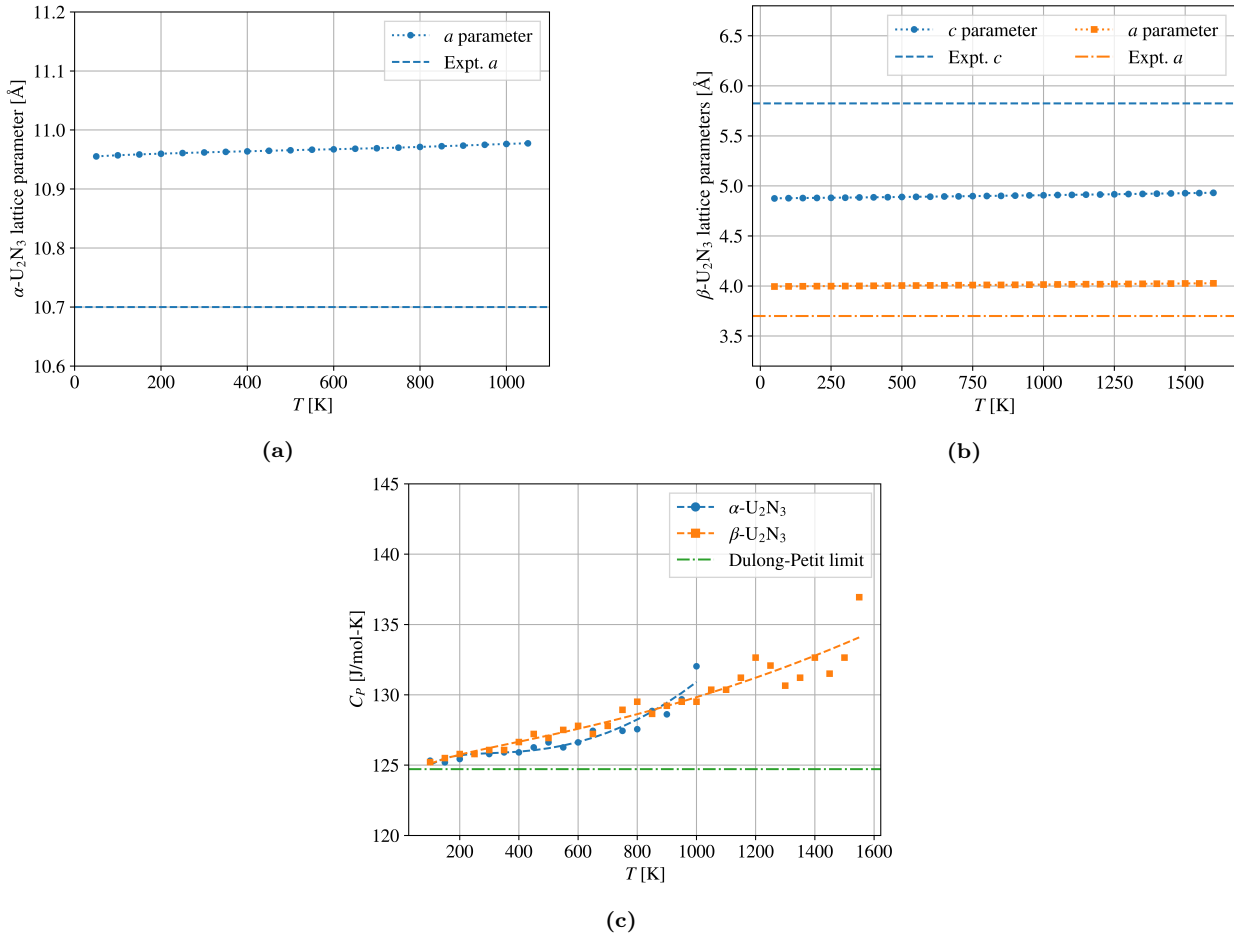


Figure B.11: The lattice parameters of (a) $\alpha\text{-U}_2\text{N}_3$, and (b) $\beta\text{-U}_2\text{N}_3$ as calculated by the Kocevski potential. (c) The specific heats of α - and $\beta\text{-U}_2\text{N}_3$ as calculated by the Kocevski potential. The curve fit of C_p of α - and $\beta\text{-U}_2\text{N}_3$ as functions of temperature are given in Eqs. (B.11) and (B.12).

- [5] A. Casagrande, L. K. Aagesen, J.-H. Ke, W. Jiang, J. D. Hales, A. Toptan, K. A. Gamble, X.-Y. Liu, S. R. Novascone, C. Matthews, D. S. Stafford, Summary of BISON milestones: NEAMS FY-20 report, Tech. rep., Idaho National Laboratory (2020).
- [6] M. Samsel-Czekała, E. Talik, P. De, R. Troć, H. Misioruk, C. Sułkowski, Electronic structure and magnetic and transport properties of single-crystalline UN, Physical Review B 76 (2007) 144426. [doi:10.1103/PhysRevB.76.144426](https://doi.org/10.1103/PhysRevB.76.144426).
- [7] R. A. Evarestov, A. I. Panin, A. V. Bandura, M. V. Losev, Electronic structure of crystalline uranium nitrides UN, U_2N_3 and UN_2 : LCAO calculations with the basis set optimization, Journal of Physics: Conference Series 117 (2008). [doi:10.1088/1742-6596/117/1/012015](https://doi.org/10.1088/1742-6596/117/1/012015).
- [8] D. Gryaznov, E. Heifets, E. Kotomin, The first-principles treatment of the electron-correlation and spin-orbital effects in uranium mononitride nuclear fuels, Physical Chemistry Chemical Physics 14 (2012) 4482–4490. [doi:10.1039/c2cp40297a](https://doi.org/10.1039/c2cp40297a).

- 696 [9] Z. G. Mei, M. Stan, B. Pichler, First-principles study of structural, elastic, electronic,
697 vibrational and thermodynamic properties of UN, Journal of Nuclear Materials 440
698 (2013) 63–69. [doi:10.1016/j.jnucmat.2013.04.058](https://doi.org/10.1016/j.jnucmat.2013.04.058).
- 699 [10] V. Kocevski, D. A. Rehn, M. W. D. Cooper, D. A. Andersson, First-principles investi-
700 gation of uranium mononitride (UN): Effect of magnetic ordering, spin-orbit inter-
701 actions and exchange correlation functional, Journal of Nuclear Materials 559 (2022).
702 [doi:10.1016/j.jnucmat.2021.153401](https://doi.org/10.1016/j.jnucmat.2021.153401).
- 703 [11] E. A. Kotomin, R. W. Grimes, Y. Mastrikov, N. J. Ashley, Atomic scale DFT simulations
704 of point defects in uranium nitride, Journal of Physics Condensed Matter 19 (2007).
705 [doi:10.1088/0953-8984/19/10/106208](https://doi.org/10.1088/0953-8984/19/10/106208).
- 706 [12] E. A. Kotomin, Y. A. Mastrikov, S. N. Rashkeev, P. V. Uffelen, Implementing first-
707 principles calculations of defect migration in a fuel performance code for UN simulations,
708 Journal of Nuclear Materials 393 (2009) 292–299. [doi:10.1016/j.jnucmat.2009.06.016](https://doi.org/10.1016/j.jnucmat.2009.06.016).
- 710 [13] D. Bocharov, D. Gryaznov, Y. F. Zhukovskii, E. A. Kotomin, DFT calculations of point
711 defects on UN(001) surface, Surface Science 605 (2011) 396–400. [doi:10.1016/j.susc.2010.11.007](https://doi.org/10.1016/j.susc.2010.11.007).
- 713 [14] J. H. Lan, Z. C. Zhao, Q. Wu, Y. L. Zhao, Z. F. Chai, W. Q. Shi, First-principles
714 DFT+*U* modeling of defect behaviors in anti-ferromagnetic uranium mononitride, Journal-
715 of Applied Physics 114 (2013). [doi:10.1063/1.4846217](https://doi.org/10.1063/1.4846217).
- 716 [15] E. A. Kotomin, Y. A. Mastrikov, First principles modeling of oxygen impurities in
717 UN nuclear fuels, Journal of Nuclear Materials 377 (2008) 492–495. [doi:10.1016/j.jnucmat.2008.04.015](https://doi.org/10.1016/j.jnucmat.2008.04.015).
- 719 [16] M. Klipfel, P. V. Uffelen, Ab initio modelling of volatile fission products in ura-
720 nium mononitride, Journal of Nuclear Materials 422 (2012) 137–142. [doi:10.1016/j.jnucmat.2011.12.018](https://doi.org/10.1016/j.jnucmat.2011.12.018).
- 722 [17] A. Claisse, M. Klipfel, N. Lindbom, M. Freyss, P. Olsson, GGA+*U* study of uranium
723 mononitride: A comparison of the U-ramping and occupation matrix schemes and incor-
724 poration energies of fission products, Journal of Nuclear Materials 478 (2016) 119–124.
725 [doi:10.1016/j.jnucmat.2016.06.007](https://doi.org/10.1016/j.jnucmat.2016.06.007).
- 726 [18] Y. J. Zhang, J. H. Lan, C. Z. Wang, Q. Y. Wu, T. Bo, Z. F. Chai, W. Q. Shi, Theoretical
727 investigation on incorporation and diffusion properties of Xe in uranium mononitride,
728 Journal of Physical Chemistry C 119 (2015) 5783–5789. [doi:10.1021/jp510219a](https://doi.org/10.1021/jp510219a).
- 729 [19] L. Yang, N. Kaltsoyannis, Incorporation of Kr and Xe in uranium mononitride: A
730 density functional theory study, Journal of Physical Chemistry C 125 (2021) 26999–
731 27008. [doi:10.1021/acs.jpcc.1c08523](https://doi.org/10.1021/acs.jpcc.1c08523).

- [20] K. Kurosaki, K. Yano, K. Yamada, M. Uno, S. Yamanaka, A molecular dynamics study of the heat capacity of uranium mononitride, *Journal of Alloys and Compounds* 297 (2000) 1–4.
- [21] K. Kurosaki, K. Yano, K. Yamada, M. Uno, S. Yamanaka, A molecular dynamics study of the thermal conductivity of uranium mononitride, *Journal of Alloys and Compounds* 311 (2000) 305–310.
- [22] P. H. Chen, X. L. Wang, X. C. Lai, G. Li, B. Y. Ao, Y. Long, Ab initio interionic potentials for UN by multiple lattice inversion, *Journal of Nuclear Materials* 404 (2010) 6–8. [doi:10.1016/j.jnucmat.2010.06.017](https://doi.org/10.1016/j.jnucmat.2010.06.017).
- [23] Y. Mishin, *Interatomic Potentials for Metals*, Springer, 2005.
- [24] A. Y. Kuksin, S. V. Starikov, D. E. Smirnova, V. I. Tseplyaev, The diffusion of point defects in uranium mononitride: Combination of DFT and atomistic simulation with novel potential, *Journal of Alloys and Compounds* 658 (2016) 385–394. [doi:10.1016/j.jallcom.2015.10.223](https://doi.org/10.1016/j.jallcom.2015.10.223).
- [25] V. I. Tseplyaev, S. V. Starikov, The atomistic simulation of pressure-induced phase transition in uranium mononitride, *Journal of Nuclear Materials* 480 (2016) 7–14. [doi:10.1016/j.jnucmat.2016.07.048](https://doi.org/10.1016/j.jnucmat.2016.07.048).
- [26] J. J. Li, S. T. Murphy, Diffusion in hypo-stoichiometric uranium mononitride, *Progress in Nuclear Energy* 142 (2021). [doi:10.1016/j.pnucene.2021.103995](https://doi.org/10.1016/j.pnucene.2021.103995).
- [27] V. Kocevski, M. W. Cooper, A. J. Claisse, D. A. Andersson, Development and application of a uranium mononitride (UN) potential: Thermomechanical properties and Xe diffusion, *Journal of Nuclear Materials* 562 (2022). [doi:10.1016/j.jnucmat.2022.153553](https://doi.org/10.1016/j.jnucmat.2022.153553).
- [28] A. P. Thompson, H. M. Aktulga, R. Berger, D. S. Bolintineanu, W. M. Brown, P. S. Crozier, P. J. in 't Veld, A. Kohlmeyer, S. G. Moore, T. D. Nguyen, R. Shan, M. J. Stevens, J. Tranchida, C. Trott, S. J. Plimpton, Lammps - a flexible simulation tool for particle-based materials modeling at the atomic, meso, and continuum scales, *Computer Physics Communications* 271 (2022). [doi:10.1016/j.cpc.2021.108171](https://doi.org/10.1016/j.cpc.2021.108171).
- [29] A. Togo, I. Tanaka, First principles phonon calculations in materials science, *Scripta Materialia* 108 (2015) 1–5. [doi:10.1016/j.scriptamat.2015.07.021](https://doi.org/10.1016/j.scriptamat.2015.07.021).
- [30] A. Carreras, A. Togo, I. Tanaka, DynaPhoPy: A code for extracting phonon quasi-particles from molecular dynamics simulations, *Computer Physics Communications* 221 (2017) 221–234. [doi:10.17632/v493dkxk8r.1](https://doi.org/10.17632/v493dkxk8r.1).
- [31] G. W. Silva, C. B. Yeamans, A. P. Sattelberger, T. Hartmann, G. S. Cerefice, K. R. Czerwinski, Reaction sequence and kinetics of uranium nitride decomposition, *Inorganic Chemistry* 48 (2009). [doi:10.1021/ic901165j](https://doi.org/10.1021/ic901165j).

- [32] S. L. Hayes, J. K. Thomas, K. L. Peddicord, Material property correlations for uranium mononitride I. physical properties, *Journal of Nuclear Materials* 171 (1990) 262–270.
- [33] S. L. Hayes, J. K. Thomas, K. L. Peddicord, Material property correlations for uranium mononitride IV. thermodynamic properties, *Journal of Nuclear Materials* 171 (1990) 300–318.
- [34] H. Tagawa, N. Masaki, X-ray and density studies of nonstoichiometric uranium sesquinitride, *Journal of Inorganic and Nuclear Chemistry* 36 (1974). [doi:10.1016/0022-1902\(74\)80220-4](https://doi.org/10.1016/0022-1902(74)80220-4).
- [35] C. E. Price, I. H. Warren, Some observations on uranium-nitrogen compounds, *Inorganic Chemistry* 4 (1965). [doi:10.1021/ic50023a028](https://doi.org/10.1021/ic50023a028).
- [36] N. Masaki, H. Tagawa, The structure of $\{\beta\text{-U}_2\text{N}_3\}$, *Journal of Nuclear Materials* 58 (1975). [doi:10.1016/0022-3115\(75\)90114-2](https://doi.org/10.1016/0022-3115(75)90114-2).
- [37] D. A. Weber, C. Schwickert, A. Senyshyn, M. Lerch, R. Pöttgen, Physical properties and lattice dynamics of bixbyite-type V_2O_3 , *Journal of Materials Research* 32 (2017). [doi:10.1557/jmr.2017.144](https://doi.org/10.1557/jmr.2017.144).
- [38] H. Okamoto, N-U (nitrogen-uranium), *Journal of Phase Equilibria* 18 (1997) 107.
- [39] S. Alavi, D. L. Thompson, Simulations of melting of polyatomic solids and nanoparticles, *Molecular Simulation* 32 (2006). [doi:10.1080/08927020600823158](https://doi.org/10.1080/08927020600823158).
- [40] Y. Zhang, E. J. Maginn, A comparison of methods for melting point calculation using molecular dynamics simulations, *Journal of Chemical Physics* 136 (2012). [doi:10.1063/1.3702587](https://doi.org/10.1063/1.3702587).
- [41] F. Ercolessi, A molecular dynamics primer, Tech. rep., International Centre for Theoretical Physics (1997).
- [42] S. J. Blundell, K. M. Blundell, Concepts in Thermal Physics, 2nd Edition, Oxford University Press, 2010.
- [43] G. Clavier, N. Desbiens, E. Bourasseau, V. Lachet, N. Brusselle-Dupend, B. Rousseau, Computation of elastic constants of solids using molecular simulation: comparison of constant volume and constant pressure ensemble methods, *Molecular Simulation* 43 (2017) 1413–1422. [doi:10.1080/08927022.2017.1313418](https://doi.org/10.1080/08927022.2017.1313418).
- [44] M. A. Meyers, K. K. Chawla, Mechanical Behavior of Materials, 2nd Edition, Cambridge University Press, 2008.
- [45] K. W. Böer, U. W. Pohl, Semiconductor Physics, Springer International Publishing AG, 2018. [doi:<https://doi.org/10.1007/978-3-319-69150-3>](https://doi.org/10.1007/978-3-319-69150-3).
- [46] O. L. Anderson, A simplified method for calculating the debye temperature from elastic constants, *Journal of Physics and Chemistry of Solids* 24 (1963) 909–917.

- 803 [47] F. Mouhat, F.-X. Coudert, Necessary and sufficient elastic stability conditions in various
804 crystal systems, Physical Review B - Condensed Matter and Materials Physics 90 (2014).
805 [doi:10.1103/PhysRevB.90.224104](https://doi.org/10.1103/PhysRevB.90.224104).
- 806 [48] D. C. Rapaport, The Art of Molecular Dynamics Simulation, 2nd Edition, Cambridge
807 University Press, 2004.
- 808 [49] H. Siethoff, K. Ahlborn, The dependence of Debye temperature on elastic constants,
809 Physica Status Solidi B 190 (1995) 179–191. [doi:10.1002/pssb.2221900126](https://doi.org/10.1002/pssb.2221900126).
- 810 [50] V. Kocevski, D. A. Rehn, A. J. Terricabras, A. van Velen, M. W. Cooper, S. W.
811 Paisner, S. C. Vogel, J. T. White, D. A. Andersson, Finite temperature properties of
812 uranium mononitride, Journal of Nuclear Materials 576 (2023) 154241. [doi:10.1016/j.jnucmat.2023.154241](https://doi.org/10.1016/j.jnucmat.2023.154241).
- 813 [51] T. R. Pavlov, M. R. Wenman, L. Vlahovic, D. Robba, R. J. Konings, P. V. Uffelen,
814 R. W. Grimes, Measurement and interpretation of the thermo-physical properties of
815 UO_2 at high temperatures: The viral effect of oxygen defects, Acta Materialia 139
816 (2017) 138–154. [doi:10.1016/j.actamat.2017.07.060](https://doi.org/10.1016/j.actamat.2017.07.060).
- 817 [52] M. S. Bryan, J. W. Pang, B. C. Larson, A. Chernatyntskiy, D. L. Abernathy, K. Gofryk,
818 M. E. Manley, Impact of anharmonicity on the vibrational entropy and specific heat of
819 UO_2 , Physical Review Materials 3 (2019). [doi:10.1103/PhysRevMaterials.3.065405](https://doi.org/10.1103/PhysRevMaterials.3.065405).
- 820 [53] R. DeHoff, Thermodynamics in Materials Science, 2nd Edition, CRC Press, 2006.
- 821 [54] E. S. R. Gopal, Specific Heats at Low Temperatures, Springer US, 1966. [doi:10.1007/978-1-4684-9081-7_4](https://doi.org/10.1007/978-1-4684-9081-7_4).
- 822 [55] J. F. Counsell, R. M. Dell, J. F. Martin, Thermodynamic properties of uranium com-
823 pounds part 2. low-temperature heat capacity and entropy of three uranium nitrides,
824 Transactions of the Faraday Society 60 (1964) 1736–1747.
- 825 [56] J. O. Scarbrough, H. L. Davis, W. Fulkerson, J. O. Betterton, Specific heat of uranium
826 mononitride from 1.3 to 4.6 K, Physical Review 176 (1968) 666–671.
- 827 [57] B. Szpunar, J. I. Ranasinghe, J. A. Szpunar, Electronic transport of uranium mononi-
828 tride, Journal of Modern Physics 12 (2021). [doi:10.4236/jmp.2021.1210084](https://doi.org/10.4236/jmp.2021.1210084).
- 829 [58] F. Giustino, Materials Modelling using Density Functional Theory: Properties and
830 Predictions, 1st Edition, Oxford University Press, 2014.
- 831 [59] E. Torres, I. CheikNjifon, T. P. Kaloni, J. Pencer, A comparative analysis of the phonon
832 properties in UO_2 using the Boltzmann transport equation coupled with DFT+ U and
833 empirical potentials, Computational Materials Science 177 (5 2020). [doi:10.1016/j.commatsci.2020.109594](https://doi.org/10.1016/j.commatsci.2020.109594).
- 834 [60] L. T. Kong, Phonon dispersion measured directly from molecular dynamics simulations,
835 Computer Physics Communications 182 (2011). [doi:10.1016/j.cpc.2011.04.019](https://doi.org/10.1016/j.cpc.2011.04.019).

- 839 [61] A. Togo, L. Chaput, I. Tanaka, Distributions of phonon lifetimes in Brillouin zones,
840 Physical Review B - Condensed Matter and Materials Physics 91 (2015). [doi:10.1103/PhysRevB.91.094306](https://doi.org/10.1103/PhysRevB.91.094306).
- 841
- 842 [62] Y. Mishin, D. Farkas, Atomistic simulation of point defects and diffusion in B2 NiAl
843 part I. point defect energetics, Philosophical Magazine A 75 (1997) 169–185. [doi:10.1080/01418619708210289](https://doi.org/10.1080/01418619708210289).
- 844
- 845 [63] C. G. V. de Walle, J. Neugebauer, First-principles calculations for defects and impurities:
846 Applications to III-nitrides, Journal of Applied Physics 95 (2004) 3851–3879. [doi:10.1063/1.1682673](https://doi.org/10.1063/1.1682673).
- 847
- 848 [64] S. Anand, J. P. Male, C. Wolverton, G. J. Snyder, Visualizing defect energetics, Materials Horizons 8 (2021) 1966–1975. [doi:10.1039/d1mh00397f](https://doi.org/10.1039/d1mh00397f).
- 849
- 850 [65] B. Dorado, M. Freyss, G. Martin, GGA+ U study of the incorporation of iodine in
851 uranium dioxide, The European Physical Journal B 69 (2009) 203–209. [doi:10.1140/epjb/e2009-00145-0](https://doi.org/10.1140/epjb/e2009-00145-0).
- 852
- 853 [66] C. Freysoldt, B. Grabowski, T. Hickel, J. Neugebauer, G. Kresse, A. Janotti, C. G. V.
854 de Walle, First-principles calculations for point defects in solids, Reviews of Modern
855 Physics 86 (2014) 253–305. [doi:10.1103/RevModPhys.86.253](https://doi.org/10.1103/RevModPhys.86.253).
- 856
- 857 [67] M. Hagen, M. W. Finnis, Determination of the atomistic structure of the $\Sigma 3$ (111) twin
858 boundary in NiAl, Materials Science Forum 207-209 (1996) 245–248. [doi:10.4028/www.scientific.net/msf.207-209.245](https://www.scientific.net/msf.207-209.245).
- 859
- 860 [68] C. Woodward, S. Kajihara, L. H. Yang, Site preferences and formation energies of
861 substitutional Si, Nb, Mo, Ta, and W solid solutions in $L1_0$ Ti-Al, Physical Review B
862 57 (1998).
- 863
- 864 [69] G. Y. Huang, G. Pastore, B. D. Wirth, First-principles study of intrinsic point defects
865 and Xe impurities in uranium monocarbide, Journal of Applied Physics 128 (2020).
866 [doi:10.1063/5.0021951](https://doi.org/10.1063/5.0021951).
- 867
- 868 [70] J. Liu, C. Gasparrini, J. T. White, K. Johnson, D. A. Lopes, V. K. Peterson, A. Studer,
869 G. J. Griffiths, G. R. Lumpkin, M. R. Wenman, P. A. Burr, E. S. Sooby, E. G. Obbard,
Thermal expansion and steam oxidation of uranium mononitride analysed via in situ
neutron diffraction, Journal of Nuclear Materials 575 (2023). [doi:10.1016/j.jnucmat.2022.154215](https://doi.org/10.1016/j.jnucmat.2022.154215).
- 870
- 871 [71] C. O. T. Galvin, N. Kuganathan, N. J. Barron, R. W. Grimes, Predicted thermo-
872 physical properties of UN, PuN, and (U,Pu)N, Journal of Applied Physics 135 (16)
873 (2024) 165101. [arXiv:https://pubs.aip.org/aip/jap/article-pdf/doi/10.1063/5.0177315/19894692/165101\1\5.0177315.pdf](https://arxiv.org/abs/https://pubs.aip.org/aip/jap/article-pdf/doi/10.1063/5.0177315/19894692/165101\1\5.0177315.pdf), [doi:10.1063/5.0177315](https://doi.org/10.1063/5.0177315).
874 URL <https://doi.org/10.1063/5.0177315>

- 875 [72] J. B. Wachtman, W. E. Tefft, D. G. Lam, C. S. Apstein, Exponential temperature
876 dependence of Young's modulus for several oxides, *Physical Review* 122 (1961) 1754–
877 1759.
- 878 [73] M. D. Salleh, J. E. Macdonald, G. A. Saunders, P. de V Du Plessis, Hydrostatic pres-
879 sure dependences of elastic constants and vibrational anharmonicity of uranium nitride,
880 *Journal of Materials Science* 21 (1986) 2577–2580.
- 881 [74] S. L. Hayes, J. K. Thomas, K. L. Peddicord, Material property correlations for uranium
882 mononitride II. mechanical properties, *Journal of Nuclear Materials* 171 (1990) 271–288.
- 883 [75] A. Padel, C. de Novion, Constantes élastiques des carbures, nitrures et oxydes d'uranium
884 et de plutonium, *Journal of Nuclear Materials* 33 (1969) 40–51.
- 885 [76] D. Frazer, B. Maiorov, U. Carvajal-Nuñez, J. Evans, E. Kardoulaki, J. Dunwoody, T. A.
886 Saleh, J. T. White, High temperature mechanical properties of fluorite crystal structured
887 materials (CeO_2 , ThO_2 , and UO_2) and advanced accident tolerant fuels (U_3Si_2 , UN, and
888 UB_2), *Journal of Nuclear Materials* 554 (2021). [doi:10.1016/j.jnucmat.2021.153035](https://doi.org/10.1016/j.jnucmat.2021.153035).
- 889 [77] C. Zener, Contributions to the theory of beta-phase alloys, *Physical Review* 71 (1947).
890 [doi:10.1103/PhysRev.71.846](https://doi.org/10.1103/PhysRev.71.846).
- 891 [78] J. Adachi, K. Kurosaki, M. Uno, S. Yamanaka, M. Takano, M. Akabori, K. Minato, Me-
892 chanical properties at sub-microscale and macroscale of polycrystalline uranium mononi-
893 tride, *Journal of Nuclear Materials* 384 (2009). [doi:10.1016/j.jnucmat.2008.09.019](https://doi.org/10.1016/j.jnucmat.2008.09.019).
- 894 [79] H. L. Whaley, W. Fulkerson, R. A. Potter, Elastic moduli and Debye temperature of
895 polycrystalline uranium nitride by ultrasonic velocity measurements, *Journal of Nuclear
896 Materials* 31 (1969). [doi:10.1016/0022-3115\(69\)90234-7](https://doi.org/10.1016/0022-3115(69)90234-7).
- 897 [80] E. F. Westrum, C. M. Barber, Uranium mononitride: Heat capacity and thermodynamic
898 properties from 5 to 350 K, *The Journal of Chemical Physics* 45 (1966) 635–639.
- 899 [81] V. G. Baranov, Y. N. Devyatko, A. V. Tenishev, A. V. Khlunov, O. V. Khomyakov, A
900 physical model for evaluating uranium nitride specific heat, *Journal of Nuclear Materials*
901 434 (2013). [doi:10.1016/j.jnucmat.2012.10.047](https://doi.org/10.1016/j.jnucmat.2012.10.047).
- 902 [82] D. P. Sellan, E. S. Landry, J. E. Turney, A. J. McGaughey, C. H. Amon, Size effects in
903 molecular dynamics thermal conductivity predictions, *Physical Review B - Condensed
904 Matter and Materials Physics* 81 (2010). [doi:10.1103/PhysRevB.81.214305](https://doi.org/10.1103/PhysRevB.81.214305).
- 905 [83] J. A. Jackman, T. M. Holden, J. I. Buyers, P. de V. DuPlessis, O. Vogt, J. Genossar,
906 Systematic study of the lattice dynamics of the uranium rocksalt-structure compounds,
907 *Physical Review B* 33 (1986) 7144–7153.
- 908 [84] A. A. Aczel, G. E. Granroth, G. J. MacDougall, W. J. Buyers, D. L. Abernathy, G. D.
909 Samolyuk, G. M. Stocks, S. E. Nagler, Quantum oscillations of nitrogen atoms in ura-
910 nium nitride, *Nature Communications* 3 (2012). [doi:10.1038/ncomms2117](https://doi.org/10.1038/ncomms2117).

- [85] N. W. Ashcroft, N. D. Mermin, Solid State Physics, 1st Edition, Cengage Learning, 1976.
- [86] X. W. Zhou, S. Aubry, R. E. Jones, A. Greenstein, P. K. Schelling, Towards more accurate molecular dynamics calculation of thermal conductivity: Case study of {GaN} bulk crystals, *Physical Review B - Condensed Matter and Materials Physics* 79 (2009). [doi:10.1103/PhysRevB.79.115201](https://doi.org/10.1103/PhysRevB.79.115201).
- [87] X. Li, P. F. Liu, E. Zhao, Z. Zhang, T. Guidi, M. D. Le, M. Avdeev, K. Ikeda, T. Otomo, M. Kofu, K. Nakajima, J. Chen, L. He, Y. Ren, X. L. Wang, B. T. Wang, Z. Ren, H. Zhao, F. Wang, Ultralow thermal conductivity from transverse acoustic phonon suppression in distorted crystalline α -MgAgSb, *Nature Communications* 11 (2020). [doi:10.1038/s41467-020-14772-5](https://doi.org/10.1038/s41467-020-14772-5).
- [88] Z. Tian, K. Esfarjani, J. Shiomi, A. S. Henry, G. Chen, On the importance of optical phonons to thermal conductivity in nanostructures, *Applied Physics Letters* 99 (2011). [doi:10.1063/1.3615709](https://doi.org/10.1063/1.3615709).
- [89] S. L. Hayes, J. K. Thomas, K. L. Peddicord, Material property correlations for uranium mononitride III. transport properties, *Journal of Nuclear Materials* 171 (1990) 289–299.
- [90] F. A. Kröger, H. J. Vink, Relations between the concentrations of imperfections in crystalline solids, *Solid State Physics - Advances in Research and Applications* 3 (1956). [doi:10.1016/S0081-1947\(08\)60135-6](https://doi.org/10.1016/S0081-1947(08)60135-6).
- [91] J. T. White, A. T. Nelson, J. T. Dunwoody, D. D. Byler, D. J. Safarik, K. J. McClellan, Thermophysical properties of U_3Si_2 to 1773 K, *Journal of Nuclear Materials* 464 (2015). [doi:10.1016/j.jnucmat.2015.04.031](https://doi.org/10.1016/j.jnucmat.2015.04.031).
- [92] Y. Lu, B. T. Wang, R. W. Li, H. L. Shi, P. Zhang, Structural, electronic, mechanical, and thermodynamic properties of UN_2 : Systematic density functional calculations, *Journal of Nuclear Materials* 410 (2011) 46–51. [doi:10.1016/j.jnucmat.2010.12.308](https://doi.org/10.1016/j.jnucmat.2010.12.308).
- [93] J. S. Olsen, L. Gerward, U. Benedict, New high-pressure phase of uranium nitride studied by X-ray diffraction and synchrotron radiation., *Journal of Applied Crystallography* 18 (1985). [doi:10.1107/S0021889885009736](https://doi.org/10.1107/S0021889885009736).
- [94] P. Modak, A. K. Verma, First-principles investigation of electronic, vibrational, elastic, and structural properties of ThN and UN up to 100 GPa, *Physical Review B - Condensed Matter and Materials Physics* 84 (2011). [doi:10.1103/PhysRevB.84.024108](https://doi.org/10.1103/PhysRevB.84.024108).
- [95] J. Rösler, H. Harders, M. Bäker, Mechanical Behaviour of Engineering Materials, Springer, 2007.
- [96] H. E. Rosinger, D. O. Northwood, The elastic properties of zirconium alloy fuel cladding and pressure tubing materials, *Journal of Nuclear Materials* 79 (1979). [doi:10.1016/0022-3115\(79\)90444-6](https://doi.org/10.1016/0022-3115(79)90444-6).
- [97] C. Kittel, Introduction to Solid State Physics, 8th Edition, John Wiley & Sons, Inc, 2005.